

1 **Title:** Drifting macrophyte detritus triggers ‘hidden’ benthic hypoxia: High metabolism and periodic
2 hypoxia associated with drifting macrophyte detritus in the shallow subtidal Baltic Sea Formatted: English (United Kingdom)

3 Formatted: English (United Kingdom)

4 **Author list:** Karl M. Attard^{1,2,3}, Anna Lyssenko³, Iván F. Rodil^{3,4}
5 **Corresponding author:** Karl M. Attard karl.attard@biology.sdu.dk Formatted: English (United Kingdom)
6 **Author affiliations:** Formatted: English (United Kingdom)

7 ¹ Department of Biology, University of Southern Denmark, 5230 Odense M, Denmark
8 ² Danish Institute for Advanced Study, University of Southern Denmark, 5230 Odense M, Denmark
9 ³ Tvärminne Zoological Station, University of Helsinki, J.A. Palménin tie 260, 10900 Hanko,
10 Finland
11 ⁴ Department of Biology (INMAR), Faculty of Marine and Environmental Sciences, University of
12 Cádiz, Puerto Real, Spain

13 **Keywords:** benthic ecosystems, primary production, respiration, oxygen fluxes, biodiversity

14 **Abstract**

15 Macrophytes form highly productive habitats that export a substantial proportion of their primary
16 production as particulate organic matter. As the detritus drifts with currents and accumulates in
17 seafloor depressions, it constitutes organic enrichment and can deteriorate O₂ conditions on the
18 seafloor. In this study, we investigate the O₂ dynamics and macrobenthic biodiversity associated
19 with a shallow ~2300 m² macrophyte detritus field in the northern Baltic Sea. The detritus,
20 primarily *Fucus vesiculosus* fragments, had a biomass of ~1700 g dry weight m⁻², approximately
21 1.5-fold larger than nearby intact *F. vesiculosus* canopies. A vertical array of O₂ sensors placed
22 within the detritus documented that hypoxia ([O₂] < 63 µmol L⁻¹) occurred for 23% of the time and
23 terminated at the onset of wave-driven hydrodynamic mixing. Measurements in five other habitats
24 nearby spanning bare sediments, seagrass, and macroalgae indicate that hypoxic conditions were
25 unique to detritus canopies. Fast-response O₂ sensors placed above the detritus documented pulses
26 of hypoxic waters originating from within the canopy. These pulses triggered a rapid short-term (~5
27 min) deterioration of O₂ conditions within the water column. Eddy covariance measurements of O₂
28 fluxes indicated high metabolic rates with that daily photosynthetic production offsetting up to 81 %

29 of the respiratory demands of the detritus canopy, prolonging its persistence within the coastal zone.
30 The detritus site had a low abundance of crustaceans, bivalves, and polychaetes when compared to
31 other habitats nearby, likely because their low-O₂ tolerance thresholds were often exceeded.

32 1. Introduction

33 Oxygen availability determines ecosystem health and the biogeochemical function of coastal waters
34 (Diaz and Rosenberg, 2008; Middelburg and Levin, 2009; Breitburg et al., 2018). When in gaseous
35 equilibrium with air, seawater typically contains an O₂ concentration ([O₂]) between 200-400 μmol
36 L⁻¹, depending on the water temperature and the salinity (Garcia and Gordon, 1992). However, both
37 abiotic and biotic processes cause significant departures from equilibrium. The main source of O₂ to
38 coastal waters is the atmosphere, where the diffusion of O₂ is governed by the air-to-sea gas
39 exchange rate (Berg and Pace, 2017; Long and Nicholson, 2018). In shallow waters and light-
40 exposed seafloor sediments, O₂ is produced by primary producers as a by-product of
41 photosynthesis, and it is consumed by consortia of microbes and fauna directly, through aerobic
42 respiration, and indirectly, through the oxidation of reduced substances (Glud, 2008). If O₂
43 consumption exceeds supply for a sufficiently long period, O₂ conditions deteriorate and become
44 hypoxic ([O₂] < 63 μmol L⁻¹). Hypoxia is becoming more common, more intense, and is affecting
45 larger areas of coastal waters, increasingly placing ecosystems and the services they provide at risk
46 (Breitburg et al., 2018). There are several well-known variants of coastal hypoxia (Diaz and
47 Rosenberg, 2008; Carstensen and Conley, 2019). Seasonal hypoxia, the most common form,
48 typically occurs in summer when warm waters, strong stratification, and high organic enrichment
49 combine to deplete O₂ until autumn (Robertson et al., 2016). Periodic O₂-depletion hypoxia, in
50 contrast, occurs more often due to local weather dynamics and tidal cycles but individual events are
51 shorter (Diaz and Rosenberg, 1995), whereas diel cycles with large day-to-night [O₂] excursions
52 trigger hypoxia for a few hours daily (Davanzo and Kremer, 1994; Tyler et al., 2009). All events are
53 expected to affect biodiversity and biogeochemical cycling to varying degrees. Seasonal and
54 periodic hypoxia and periodic O₂-depletion are associated with large-scale mortality of organisms
55 and a switch between retention and removal of bioavailable nutrients such as nitrate, ammonium,
56 phosphate, and toxic hydrogen sulfide (Middelburg and Levin, 2009; Carstensen and Conley,
57 2019). Short-term hypoxic events hypoxia can similarly exceed lethal and non-lethal thresholds for
58 many benthic taxa (Vaqueiro-Sunyer and Duarte, 2008), although, due to their sporadic nature, their
59 occurrence and impacts are less understood.

Formatted: English (United Kingdom)

60 Given the importance of O₂ in coastal waters, [O₂] is one of the most frequently measured
61 environmental parameters. Near-seabed [O₂ availability] is typically measured using long-term
62 stable O₂ sensors (e.g. optodes, (Bittig et al., 2018)) that are moored ~0.35-1.0 m above the
63 seafloor, or by performing vertical profiles of water column [O₂] down to ~1.0 m above the seafloor
64 using multiparameter sondes. National monitoring programs such as those maintained by the
65 Swedish Meteorological and Hydrological Institute and the Finnish Environment Institute provide a
66 wealth of essential open-access data, enabling important analyses detailing the prevalence and
67 intensity of coastal hypoxia (Virtanen et al., 2019; Conley et al., 2011; Carstensen and Conley,
68 2019). Notwithstanding the progress being made in coastal monitoring, it was demonstrated more
69 than 40 years ago that the largest [O₂] gradients may occur just a few cm above the seafloor due to
70 the high reactivity of marine sediments and a strong benthic O₂ demand (Jorgensen, 1980). To date,
71 records of hypoxia in the shallow subtidal zone are still somewhat scarce. In a compilation of
72 monitoring data for the northern Baltic Sea (Gulf of Finland and Archipelago Sea), Virtanen et al.
73 (2019), found that just 11 out of 461 (or 2.4%) of the monitoring stations that registered hypoxia
74 occurred in waters < 5 m depth. While this may reflect a true signal that hypoxia is more
75 widespread in deeper coastal waters, it is also likely that hypoxic conditions affecting the seafloor
76 may therefore remain 'hidden' go undetected if measurements sensors are located performed away
77 from the seafloor, higher up in the water column, as is common practice (Conley et al., 2011;
78 Virtanen et al., 2019).

79 Around two-thirds of the ocean's photosynthetic biomass is bound in macrophytes growing in
80 shallow waters along the world's coastline (Smith, 1981). Through seasonal decay, epiphyte
81 growth, grazing, and physical forcing (e.g. waves, currents, ice scouring), macrophytes export a
82 large proportion of their primary production (~40 %) to their surroundings as detritus (Attard et al.,
83 2019a; Krumhansl and Scheibling, 2012; Duarte and Cebrián, 1996). Macrophyte detritus drifts
84 with the currents and accumulates on the shoreline and in low-energy marine environments (e.g.
85 shallow seafloor depressions and in deeper waters), where it constitutes habitat structure and
86 organic enrichment to the receiving habitat (Norkko and Bonsdorff, 1996b). Given high enough
87 abundance, detritus suppresses the diffusion of O₂ from the water column to the sediment surface
88 and it exacerbates O₂ depletion on the seabed as it decays. Large accumulations of unattached
89 ephemeral macroalgae such as the brown algae *Ectocarpus siliculosus* and *Pylaiella littoralis* are
90 common in eutrophic coastal waters such as the Baltic Sea, forming thin mats above the seafloor
91 typically a few centimeters thick (Norkko and Bonsdorff, 1996a). While coastal hypoxia is most

Formatted: English (United Kingdom)

92 commonly associated with eutrophic waters such as the Baltic Sea (Carstensen and Conley, 2019;
93 Conley et al., 2011), hypoxic (and even sulfidic) conditions have been reported in remote and more
94 pristine environments such as the high Arctic due to large accumulations of detritus produced
95 from perennial brown seaweeds have also been observed (Glud et al., 2004). However, the O₂
96 dynamics within accumulations of drifting detritus and the potential implications for the associated
97 fauna remain poorly understood. Understanding the ecological and biogeochemical implications of
98 drifting macrophyte detritus is particularly important given the ambitions to vastly increase
99 macroalgal farming (Broch et al., 2019), which would result in increased deposition of macrophyte
100 detritus on the coastal seafloor (Broch et al., 2022).

101 In this study, we investigate the O₂ dynamics and macrobenthic biodiversity associated with a
102 shallow ~2300 m² macrophyte detritus field composed of *Fucus vesiculosus* fragments in the
103 northern Baltic Sea. To assess O₂ production versus consumption rates of the detritus canopy, we
104 deployed an eddy covariance system on multiple occasions to extract benthic O₂ fluxes non-
105 invasively. Using a vertical array of O₂ sensors and an acoustic velocimeter, we monitored O₂
106 distribution within the canopy and the hydrodynamics above the canopy to assess the occurrence
107 and intensity of hypoxic events and their links to local hydrodynamics. We performed biodiversity
108 surveys to identify the prevailing taxa, and we compared hypoxic thresholds of these taxa to [O₂]
109 measured *in situ* to identify potential stress. Measurements were also performed in five other
110 habitats nearby spanning bare sediments, seagrass, and macroalgae for comparison.

111 2. Materials and Methods

112 2.1. Study location

113 The study was performed in the microtidal Baltic Sea nearby the Tvärminne Zoological Station in
114 SW Finland. Although the focus of our study was to investigate drifting macrophyte detritus, we
115 selected an additional five study sites within the shallow subtidal zone (2–4 m depth) for
116 comparison, representing key habitats in the Baltic Sea: one site with bare sediments, two sites with
117 seagrass (predominantly *Zostera marina*; sheltered and exposed), and two sites with intact
118 macroalgae canopies (predominantly *Fucus vesiculosus*; sheltered and exposed) (Table 1).

Site	Location	Deployment start	Deployment duration (h)	Water depth (m)	Water temperature (°C)	Minimum O ₂ (μmol L ⁻¹)	Maximum O ₂ (μmol L ⁻¹)	Hypoxia duration (h)
------	----------	------------------	-------------------------	-----------------	------------------------	--	--	----------------------

Macrophyte detritus	59 811613 N 23 206624 E	29-05-2018	- - - 120 - - -	- 3.0 -	- - 12 - - -	- - 0.6 - - -	- - - 429 - - -	- - - 27 - - -	Formatted: English (United Kingdom)
Bare sediments	59 841532 N 23 253370 E	20-05-2018	- - - 96 - - -	- 3.7 -	- - 11 - - -	- - 307 - - -	- - - 407 - - -	- - - 0 - - -	Formatted: English (United Kingdom)
Sheltered Z. marina	59 841551 N 23 251203 E	27-05-2018	- - - 87 - - -	- 4.0 -	- - 16 - - -	- - 272 - - -	- - - 333 - - -	- - - 0 - - -	Formatted: English (United Kingdom)
Exposed Z. marina	59 827008 N 23 151976 E	08-06-2018	- - - 120 - - -	- 2.9 -	- - 10 - - -	- - 281 - - -	- - - 437 - - -	- - - 0 - - -	Formatted: English (United Kingdom)
Sheltered F. vesiculosus	59 826856 N 23 209721 E	08-06-2018	- - - 120 - - -	- 2.0 -	- - 10 - - -	- - 253 - - -	- - - 489 - - -	- - - 0 - - -	Formatted: English (United Kingdom)
Exposed F. vesiculosus	59 811359 N 23 207281 E	3101-056-2018	- - - 116 - - -	- 2.0 -	- - 9 - - -	- - 287 - - -	- - - 427 - - -	- - - 0 - - -	Formatted: English (United Kingdom)

119 Table 1: Environmental conditions and low-oxygen events at the six study sites Formatted: English (United Kingdom)

120

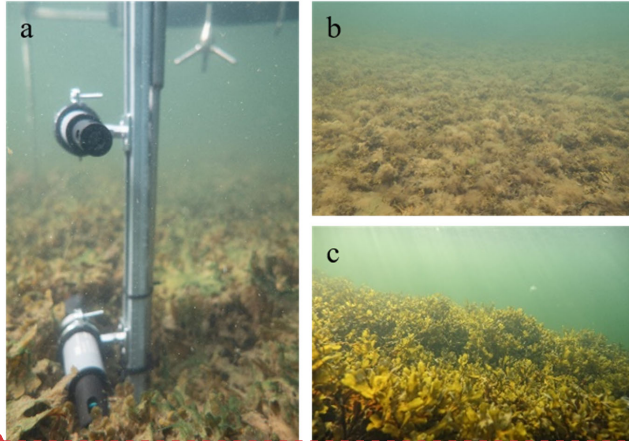
121 2.2. $[O_2]$ dynamics in benthic habitats Formatted: English (United Kingdom)

122 To investigate the near-bed $[O_2]$ dynamics and its environmental controls, we equipped a tripod
123 frame with a suite of sensors consisting of three cross-calibrated dissolved $[O_2]$ -loggers with inbuilt
124 temperature compensation (HOBO U26-001, Onset), a 6 MHz acoustic velocimeter (Vector,
125 Nortek), a photosynthetic active radiation (PAR) sensor (RBRsolo with Licor PAR Quantum

126 192SA), and a saltwater conductivity sensor (HOBO U24-002-C). The $[O_2]$ -loggers have a factory-
127 specified accuracy of $\pm 6 \mu\text{mol L}^{-1}$ from 0 to $250 \mu\text{mol L}^{-1}$, $\pm 16 \mu\text{mol L}^{-1}$ from 250 - $625 \mu\text{mol L}^{-1}$, a
128 resolution of $0.6 \mu\text{mol L}^{-1}$ and a 90% response time (T_{90}) < 2 min. The $[O_2]$ -and conductivity
129 sensors were mounted onto a 75 cm-long stainless steel rail affixed to the tripod leg
130 (Fig. 1). The sensors were secured to the rail at various heights above the seabed using rail mount
131 clamps. For the study sites with canopies, two sensors were set inside the canopy; one sensor was
132 ~ 5 cm above the seafloor and one was close to the top of the canopy (15-25 cm). The third sensor
133 was placed in the water above the canopy (~ 35 cm above the seafloor). The tripod was deployed by
134 divers from a small boat and was carefully positioned on the seafloor using a lift bag. The exact
135 sensor heights were noted by the divers once the instrument was on the seafloor. The instrument
136 was left to record data for 3-5 days at each site. The velocimeter sampled three-dimensional flow
137 velocity continuously at 8 Hz, whereas the $[O_2]$, temperature, conductivity, and PAR sensors
138 recorded data every minute. Formatted: English (United Kingdom)

139 To investigate $[O_2]$ -dynamics and its environmental drivers, all sensor time series were aligned in
140 time and analyses were performed to investigate vertical gradients in O_2 distribution, diel $[O_2]$
141 excursions, and boundary-layer hydrodynamics. We assessed the occurrence of hypoxia ($[O_2] < 63$
142 $\mu\text{mol L}^{-1}$) by quantifying the magnitude (lowest $[O_2]$ -value) and the duration (in hours) of hypoxic
Formatted: English (United Kingdom)

143 events. The high-frequency velocity data were used to calculate mean flow velocity magnitude (\bar{U})
144 as the sum of streamwise (u) and traverse (v) components, as $\bar{U} = \sqrt{u^2 + v^2}$.



145
146 Fig. 1: The study area showing (a) the instrument deployed within the detritus canopy, (b) a broad-
147 scale view of the detritus accumulation area, and (c) a nearby intact *Fucus vesiculosus* canopy.

Formatted: English (United Kingdom)

Formatted: English (United Kingdom)

148 2.3. Benthic O_2 fluxes

149 An aquatic eddy covariance system was deployed at the detritus site to quantify benthic O_2 fluxes at
150 the canopy-water interface on three occasions (June 2017, September 2017, and May 2018). Eddy
151 covariance integrates over a relatively large seafloor area (typically $\sim 30 \text{ m}^2$) (Berg et al., 2007) and
152 extracts fluxes without disturbing the hydrodynamics or the light, which is particularly useful when
153 trying to understand the mechanistic drivers of $[O_2]$ dynamics (Berg et al., 2022). The eddy
154 covariance setup was identical to the tripod frame described above, with the addition of a fast-
155 response ($T_{90} < 0.3 \text{ s}$) $[O_2]$ -microsensor setup for covariance measurements (McGinnis et al.,
156 2011). The hardware and data processing techniques are described in detail in Attard et al. (2019b).
157 This instrument can capture the entire range of flux-contributing turbulent eddies within the benthic
158 boundary layer, and this information is used to approximate the benthic O_2 flux non-invasively
159 (Berg et al., 2003; Berg et al., 2022). The instrument recorded co-located measurements of the
160 vertical velocity (w) and the O_2 concentration (C) at 32 Hz, and the data were processed using a
161 multiple-step protocol detailed in Attard et al. (2019b) to extract and quality-check benthic fluxes.
162 In short, the data streams for w and C were decomposed into mean and fluctuating components

Formatted: English (United Kingdom)

Formatted: Superscript

Formatted: Subscript

Formatted: English (United Kingdom)

163 using Reynolds decomposition, as $w = \bar{w} + w'$ and $C = \bar{C} + C'$ (Berg et al., 2003). The turbulent
 164 flux (J_{EC}) was then computed in units of $\text{mmol O}_2 \text{ m}^{-2} \text{ h}^{-1}$ as $J_{EC} = \overline{w' C'}$, where the overbar
 165 represents a period of 15 min. The turbulent flux was then summed with a storage correction term to
 166 calculate the total benthic flux (J_{benthic} , $\text{mmol O}_2 \text{ m}^{-2} \text{ h}^{-1}$) (Rheuban et al., 2014), as:

$$J_{\text{benthic}} = J_{EC} + \int_0^h \frac{\partial C}{\partial t} dz$$

167
 168 The storage correction term was defined using the three $[\text{O}_2]$ optodes placed within and above the
 169 canopy. For the correction, as we defined a matrix with the number of rows n corresponding to the
 170 sensor measurement height above the seafloor (1 row per cm) (Camillini et al., 2021). To do this,
 171 the oxygen time series, consisting of $[\text{O}_2]$ measurements performed at three heights within the
 172 canopy, were converted to a matrix using the software package OriginPro 2022. Since the
 173 measurement height of the three sensors were spaced nonlinearly, the data were first converted to
 174 XYZ column format using the w2xyz function. Next, the three rows, representing the $[\text{O}_2]$ time
 175 series measurements at three heights, were expanded to n rows, with n representing the sensor
 176 measurement height in cm (from 0 to n cm above seabed, 1 row per cm) using the XYZ Gridding
 177 function. This generated a matrix of n rows consisting of linearly interpolated $[\text{O}_2]$. Interpolation
 178 was performed using the Random (Renka Cline) gridding method. Next, a storage correction term
 179 was calculated for each 1 cm cell as described by Rheuban et al. (2014), and the total storage
 180 correction was subsequently computed for the water volume below the sensor measurement height
 181 as the sum of the n rows, an average of the O_2 sensors located within and above the canopy
 182 (Camillini et al., 2021). The high-frequency $[\text{O}_2]$ time series from the fast-response microsensors
 183 were also analyzed to identify any pulses of low $[\text{O}_2]$ -waters originating from within the canopy
 184 and propagating upwards into the water column.

185 2.4. Benthic metabolic rates

186 The O_2 flux time series was separated into individual 24 h periods (midnight to midnight). The
 187 daytime flux (Flux_{day} , $\text{mmol O}_2 \text{ m}^{-2} \text{ h}^{-1}$) was computed as a bulk average of fluxes measured when
 188 $\text{PAR} > 1.0 \mu\text{mol m}^{-2} \text{ s}^{-1}$. The nighttime flux ($\text{Flux}_{\text{night}}$, $\text{mmol O}_2 \text{ m}^{-2} \text{ h}^{-1}$) was calculated as the
 189 average of the remaining fluxes, when $\text{PAR} < 1.0 \mu\text{mol m}^{-2} \text{ s}^{-1}$. These two values and the number of
 190 daylight hours (h_{day}) were used to estimate the daily photosynthetic rate, termed the gross primary
 191 production (GPP , in $\text{mmol O}_2 \text{ m}^{-2} \text{ d}^{-1}$), as $GPP = \text{Flux}_{\text{day}} + \text{abs}(\text{Flux}_{\text{night}}) * h_{\text{day}}$, and daily
 192 respiration (R , in $\text{mmol O}_2 \text{ m}^{-2} \text{ d}^{-1}$), as $R = \text{abs}(\text{Flux}_{\text{night}}) * 24$, assuming a light-independent

Formatted

[2]

Formatted

[3]

Formatted

[4]

Formatted

[5]

Formatted

[1]

Formatted

[6]

Formatted

[7]

Formatted

[8]

193 respiration rate. The latter is a common assumption, but it is known that it underestimates the true
194 metabolic activity (Fenchel and Glud, 2000; Juska and Berg, 2022). The daily balance between
195 GPP and R , termed the net ecosystem metabolism (NEM , in $\text{mmol O}_2 \text{ m}^{-2} \text{ d}^{-1}$) was estimated as
196 $NEM = GPP - R$ (Attard et al., 2019b).

Formatted: English (United Kingdom)

197 The relationship between seafloor PAR and the in situ benthic O_2 flux was investigated using light-
198 saturation curves. Hourly O_2 fluxes were plotted against the corresponding near-bed incident PAR
199 and the relationship between the two was investigated using a modified tangential hyperbolic
200 function by Platt et al. (1980), as $O_2 \text{ flux} = P_m * \tanh\left(\frac{\alpha I}{P_m}\right) - R$, where P_m is the maximum rate of
201 hourly gross primary production, α is the initial quasi-linear increase in O_2 flux with PAR, I is near-
202 bed irradiance (PAR), and R is the dark respiration rate. The photosaturation parameter, I_k (μmol
203 $\text{PAR m}^{-2} \text{ s}^{-1}$) was derived as P_m/α . Non-linear curve fitting was performed in OriginPro 2022b
204 using a Levenberg–Marquardt iteration algorithm, until a Chi-Squared tolerance value of 1E-9 was
205 reached (Attard and Glud, 2020).

Formatted: English (United Kingdom)

Formatted: English (United Kingdom)

206 2.5. Biodiversity sampling

207 At all six sites, we aimed to obtain a quantitative understanding of the abundance, biomass, and
208 species richness of macrophytes and macrofauna (infauna and epifauna). The different habitats
209 required different sampling strategies, since four sites were sedimentary (bare sediments site, two
210 seagrass sites, and the detritus sites) and two sites were rocky (two macroalgal sites) (Rodil et al.,
211 2019).

Formatted: English (United Kingdom)

212 At the time of our study, the detritus site had a ~20-cm thick detritus mat covering the seabed
213 sediments. The detritus canopy was sampled using large stainless steel core liners (inner diameter =
214 19 cm; $n = 4$) capable of cutting through the mat, and the collected samples were transferred into a
215 fine-mesh bag. In the laboratory, the detritus was rinsed through a 0.5 mm sieve to collect the
216 associated epifauna. Samples of algal detritus were dried at 60°C for 48 hours and the biomass was
217 calculated as dry weight / m^2 .

218 Macrofauna at the four sedimentary habitats was sampled using six sediment cores (inner
219 diameter = 5.0 cm, depth = 15 cm). The samples were sieved through a 0.5 mm sieve and animals
220 were stored in alcohol for later identification. At the seagrass sites, representative macrophyte
221 samples were collected by divers from an area around the tripod frame at the end of the deployment
222 using four randomly-placed quadrats (20 x 20 cm). The seagrass within each quadrat was gently

223 uprooted and was transferred into a net-bag. In the laboratory, the samples were rinsed through a
224 0.5 mm sieve to collect all the associated epifauna. The animals were stored in alcohol for later
225 identification, and the seagrass was frozen in sealed bags for further processing. The seagrass
226 samples were later thawed, ~~and the length (cm) of each shoot was measured to determine the~~
227 ~~average length of the canopy. I, and~~ individual shoots were counted to determine the canopy density
228 in m². The above- and below-ground macrophyte biomass was separated, dried at 60°C for 48 hours
229 and weighed.

230 At the rocky sites, *F. vesiculosus* individuals ($n = 4$) were randomly collected from around the
231 instrument in fine-mesh bags. Randomly-placed quadrats (1 m², $n = 4$) were used to quantify the
232 number of *F. vesiculosus* individuals per m². At the laboratory, the collected *F. vesiculosus* samples
233 were carefully rinsed through a 0.5 mm sieve to collect the epifauna. The height of the *F.*
234 *vesiculosus* canopy was determined from the average length of the sampled individuals. Both *F.*
235 *vesiculosus* and epiphytes were separated to the extent possible, dried at 60 °C for 48 h and
236 weighed. To collect any macrofauna on the bare rock beneath the *F. vesiculosus* canopy, Kautsky-
237 type samplers were placed on the seafloor and the 20 cm x 20 cm area was gently scraped using a
238 spoon into a fine-mesh sampling bag. In the laboratory, all the macrofauna from the four replicates
239 were sieved through a 0.5 mm sieve and stored in alcohol.

240 The fauna from all habitats was sorted, identified to species level, counted, and weighed. The wet
241 weight for each species was noted with 0.0001 g accuracy. In cases where the fauna occurred in
242 very high numbers, the sample was placed in a water-filled tray and divided into eight sectors. Four
243 sectors were randomly chosen to calculate abundance and biomass. The length of gastropods and
244 bivalves was measured from anterior to posterior axis using Vernier callipers (~~accuracy = 0.01 mm~~)
245 for conversion to ash-free dry mass (AFDM). The AFDM of bivalves and gastropods was
246 calculated using established relationships between length and weight for Baltic Sea fauna (~~Rumohr~~
247 et al., 1987).

Formatted: English (United Kingdom)

Formatted: English (United Kingdom)

Formatted: English (United Kingdom)

248 The abundance (ind m⁻²) and biomass (AFDM/SFDM g m⁻²) of the invertebrates across sites were
249 calculated. Primer (v.7 and PERMANOVA+) software was used to perform the nonmetric
250 multidimensional scaling (nMDS, with fourth-root-transformed data) to visualize macrofauna
251 assemblages between sites. ANOSIM based on the Bray-Curtis similarity matrix was also
252 performed in Primer (site as a fixed factor, 4999 random sample permutations) to compare
253 differences in macrofauna abundance and biomass between sites.

254

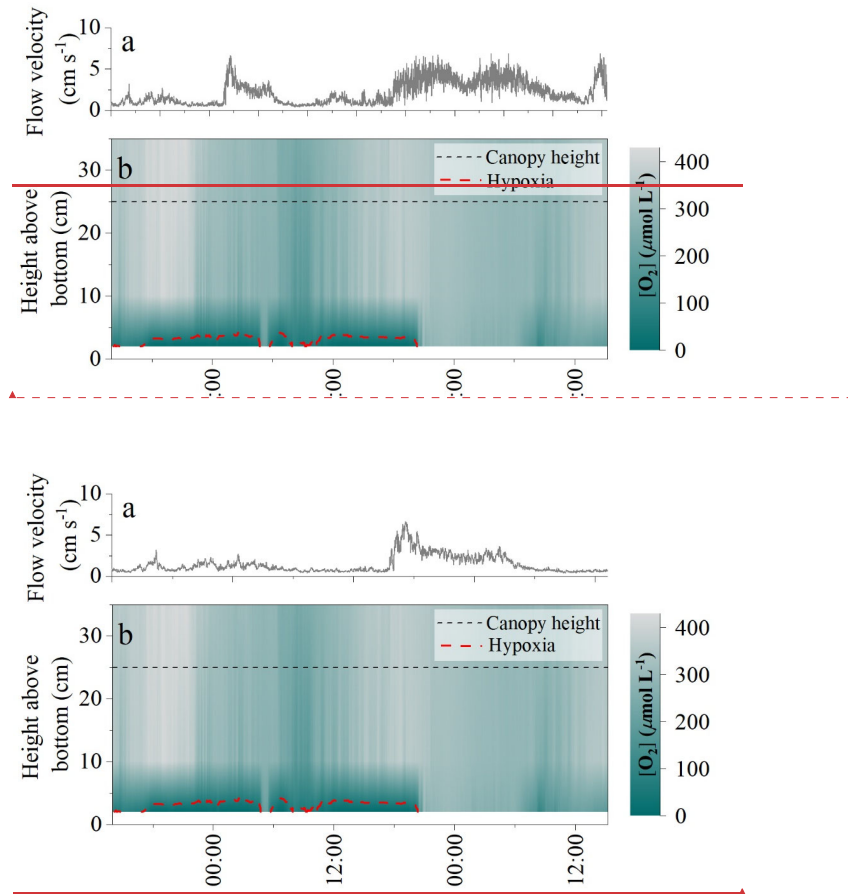
255 **3. Results**

256 *3.1. Environmental conditions*

257 Average water depth ranged from 2.0 m to 4.0 m at the six study sites, and average water
258 temperature ranged from 9 °C to 16 °C during the study period (Table 1). Hypoxic conditions were
259 only detected at the detritus site. Bottom-water $[O_2]$ at the detritus site ranged from 1 $\mu\text{mol L}^{-1}$ to
260 429 $\mu\text{mol L}^{-1}$, with hypoxic conditions occurring for 27 h out of the 120 h long deployment (i.e. for
261 23 % of the time) (Table 1). At the five other measurement sites, $[O_2]$ were well above hypoxic
262 conditions, with overall concentrations following diel patterns and ranging from 250 $\mu\text{mol L}^{-1}$ to
263 490 $\mu\text{mol L}^{-1}$ (Table 1).

264 *3.2. $[O_2]$ dynamics* *Oxygen dynamics* in detritus canopies

265 The $[O_2]$ *oxygen* measurements within the detrital canopy document a highly dynamic $[O_2]$
266 environment driven by light availability and flow velocity (Fig. 2). Within the upper layers of the
267 canopy (i.e. ~10 to 25 cm above the seafloor), $[O_2]$ and temporal dynamics largely follow diel
268 patterns driven by light availability, with large ~250 $\mu\text{mol L}^{-1}$ diel excursions in $[O_2]$. *In the upper*
269 *canopy region* *There*, the $[O_2]$ was lowest in the morning (~160 $\mu\text{mol L}^{-1}$) and highest in the evening
270 (~430 $\mu\text{mol L}^{-1}$). In all cases, $[O_2]$ within the upper canopy region was above hypoxic thresholds.
271 However, under low average flow velocities < 2 cm s^{-1} , $[O_2]$ within the lower canopy region (< 10
272 cm) deviated substantially from the conditions above. No diel variations in $[O_2]$ *were observed*
273 during these periods, and $[O_2]$ rapidly became hypoxic for sustained periods (> 24 h long), with
274 $[O_2]$ being very low (< 10 $\mu\text{mol L}^{-1}$) during ~10 hr (~8 % of the time) (Fig. 2). As hypoxia persisted
275 throughout the night under low flow velocities, low $[O_2]$ extended upwards into the canopy.
276 Hypoxic conditions ended at the onset of higher mean flow velocities of ~7 cm s^{-1} , which initiated a
277 rapid (i.e. within 1.5 hr) oxygenation of the entire canopy.



278 Fig. 2: (a) Flow velocity measured by the velocimeter 10 cm above the detritus canopy and (b) O₂
279 distribution within the canopy as resolved by three O₂ sensors located at 3 cm, 10 cm, and 35 cm
280 above the seafloor. Deployment starting from 29th May 2018.

281 *3.3. Pulses of hypoxic waters*

282 High-frequency [O₂]-measurements performed 10 cm above the detritus canopy document transient
283 pulses of hypoxic water originating from within the canopy and propagating upwards into the water
284 column (Fig 3). Such pulses typically followed quiescent weather and occurred at the onset of
285 increased flow velocities. It took < 1 min to reduce [O₂] in the water column from 220 μmol L⁻¹ to

286 Formatted: English (United Kingdom)

287 Formatted: English (United Kingdom)

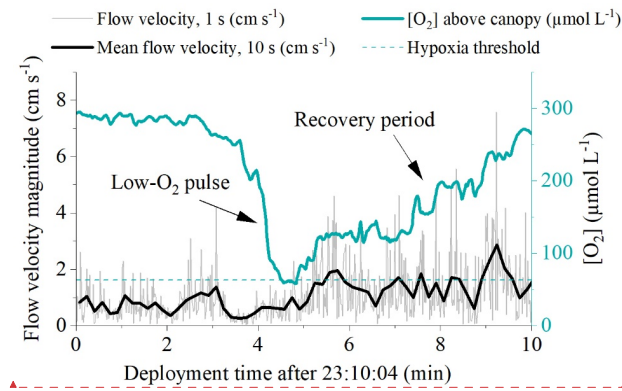
288 Formatted: Superscript

289 Formatted: English (United Kingdom)

290 Formatted: English (United Kingdom)

288 65 $\mu\text{mol L}^{-1}$. Subsequently, a recovery period followed where $[\text{O}_2]$ gradually increased back to
289 previous concentrations over a \sim 5 min period. These rapid variations in water column $[\text{O}_2]$ were not
290 captured by the slow-response $[\text{O}_2]$ -optode sampling at 1 min intervals.

Formatted: English (United Kingdom)



291
292 Figure 3: High-frequency $[\text{O}_2]$ measured 10 cm above the detrital canopy documented pulses of
293 hypoxic water originating from within the canopy and propagating upwards into the water column.

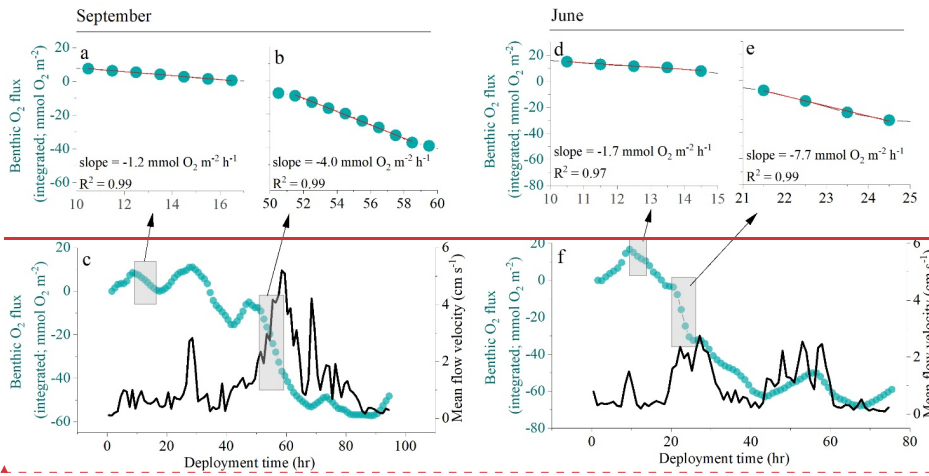
294 Data from 20th September 2017.

Formatted: Superscript

Formatted: English (United Kingdom)

296 3.4. Benthic O_2 fluxes and detritus metabolic rates

297 The eddy covariance measurements at the detritus site produced three days of continuous flux data
298 in June 2017, three days of data in September 2017, and five days of data in June-May 2018.
299 Benthic O_2 fluxes documented a dynamic O_2 exchange rate driven by light availability and flow
300 velocity (Fig. 4). During quiescent periods with low flow velocity $< 2 \text{ cm s}^{-1}$, a clear diel signal in
301 the O_2 flux was observed, indicating substantial primary production associated to the detritus
302 canopy. Higher flow velocities stimulated O_2 uptake rates by up to 5-fold, indicating that canopy
303 ventilation through mixing increased O_2 uptake (Fig. 4).



304
305 **Fig 4: Eddy covariance O₂ fluxes measured 10 cm above the canopy in September (a-c) and June**
306 **(d-f).** Oxygen consumption rates during quiescent periods (panels a and d) were 3.3 and 4.5 fold
307 **lower than fluxes measured during more turbulent periods (panels b and e), indicating that canopy**
308 **ventilation through mixing stimulated O₂ uptake.**

310 Hourly O₂ fluxes ranged from -22 mmol O₂ m⁻² h⁻¹ at night to 13 mmol O₂ m⁻² h⁻¹ during the day
311 and showed a distinct diel cycle in response to sunlight availability (Fig. 4S). Daily R ranged from
312 26 to 97 mmol O₂ m⁻² d⁻¹, and daily GPP was between 15 and 74 mmol O₂ m⁻² d⁻¹. Daily R
313 exceeded GPP in all 11 measurement days (net heterotrophic), with NEM ranging from -7 to -32
314 mmol O₂ m⁻² d⁻¹ (Fig. 4, Table A15). The deployment average (\pm SD) GPP:R for the detritus
315 canopy was 0.77 ± 0.04 in June 2017 ($n = 3$), 0.55 ± 0.02 in September 2017 ($n = 3$), and $0.77 \pm$
316 0.00 in June May 2018 ($n = 5$), and the global mean GPP:R was 0.71 ± 0.11 ($n = 11$).

317 There was a significant positive relationship between daily detritus GPP and R in all measurement
318 campaigns, with the detritus canopy seemingly becoming more heterotrophic (i.e. R > GPP) as the
319 magnitude of the metabolic rates increased (Fig. 5, Table A1). Significant positive relationships
320 were also observed between daily detritus GPP and daily seabed PAR (Table A1). Canopy light-use
321 efficiency (LUE), estimated as the ratio between daily GPP and daily PAR (Attard and Glud, 2020)
322 was 0.004 O₂ photon⁻¹ in June 2017, 0.006 O₂ photon⁻¹ in September 2017, and 0.004 O₂ photon⁻¹ in
323 May 2018 (Table A1).

Formatted: English (United Kingdom)

Formatted: Left

Formatted: English (United Kingdom)

Formatted: English (United Kingdom)

Formatted: English (United Kingdom)

Formatted: English (United Kingdom), Subscript

Formatted: English (United Kingdom)

Formatted: English (United Kingdom), Superscript

Formatted: English (United Kingdom)

Formatted: English (United Kingdom), Subscript

Formatted: English (United Kingdom)

Formatted: English (United Kingdom), Superscript

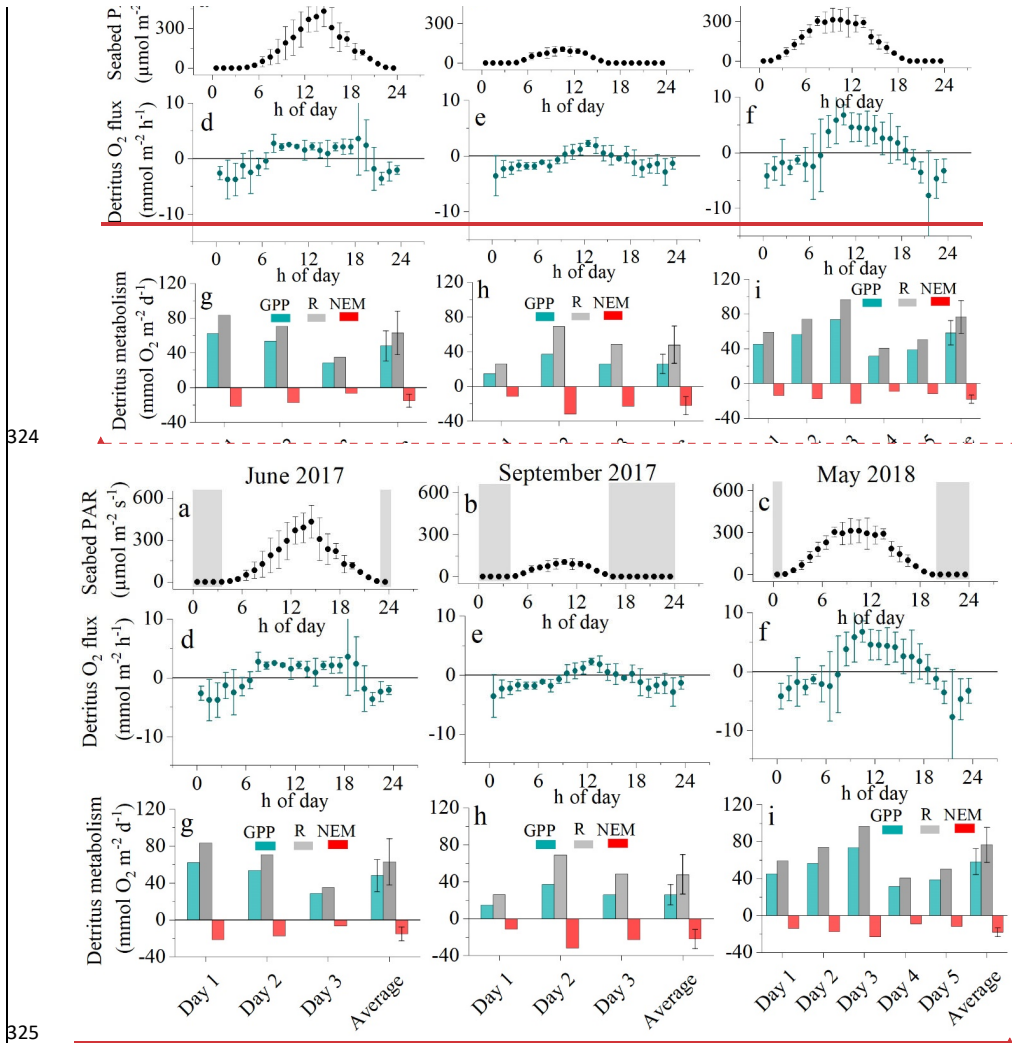
Formatted: English (United Kingdom)

Formatted: English (United Kingdom), Subscript

Formatted: English (United Kingdom)

Formatted: English (United Kingdom), Superscript

Formatted: English (United Kingdom)



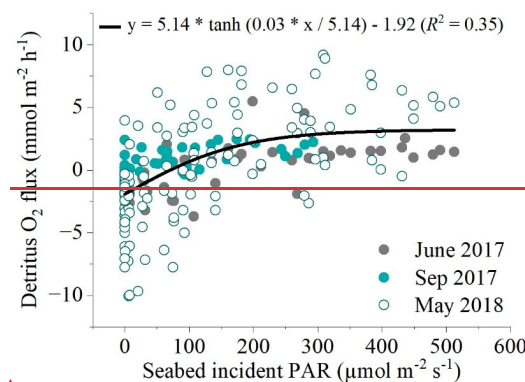
326 Fig. 45: Hourly seabed PAR (a, b, c) with night-time periods grey shaded, hourly O_2 fluxes (d, e, f)
 327 and daily metabolism estimates of gross primary production (GPP), respiration (R), and net
 328 ecosystem metabolism (NEM) for the detritus canopy (b, d, f) for the three measurement campaigns
 329 (g, h, i). Seabed PAR and O_2 fluxes are shown as mean \pm 1 s.d. and are binned by the hour of day.

330 Formatted: English (United Kingdom)

330 Formatted: English (United Kingdom), Subscript

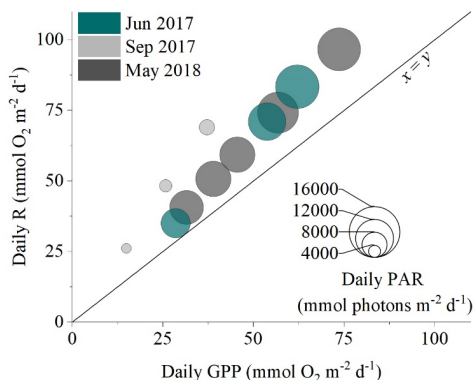
330 Formatted: English (United Kingdom)

331 There was a significant positive relationship between near-bed incident PAR and the benthic O₂
 332 flux (Fig. 56). Light-saturation curves fitted to hourly data from all deployments indicated a
 333 maximum gross primary production rate (P_m) of $5.14 \pm 0.56 \text{ mmol O}_2 \text{ m}^{-2} \text{ h}^{-1}$, an α of 0.03 ± 0.01 ,
 334 and a R rate of $1.92 \pm 0.26 \text{ mmol O}_2 \text{ m}^{-2} \text{ h}^{-1}$. Light saturation (I_k) of the detritus canopy occurred at
 335 irradiances greater than $\sim 170 \text{ } \mu\text{mol PAR m}^{-2} \text{ s}^{-1}$.



Formatted: English (United Kingdom)

336
 337 Fig. 6: Relationship between all hourly in situ benthic O₂ fluxes at the detritus site and light
 338 availability from the three flux datasets measured. A modified photosynthesis-irradiance curve by
 339 Platt et al. (1980) is shown together with 95% confidence bands.

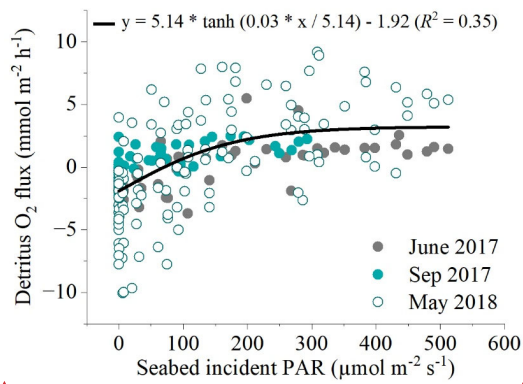


Formatted: English (United Kingdom)

Formatted: English (United Kingdom)

Formatted: Centered

340
 341 Fig. 5: The daily balance between detritus gross primary production (GPP) and respiration (R) for the
 342 three measurement campaigns. Symbol size corresponds to the daily integrated PAR reaching the
 343 seafloor.



Formatted: English (United Kingdom)

Formatted: English (United Kingdom)

344
345 Fig. 6: Relationship between all hourly in situ benthic O₂ fluxes at the detritus site and light
346 availability from the three flux datasets measured. A modified photosynthesis-irradiance curve by
347 Platt et al. (1980) is shown as the line-of-best-fit to the global dataset.

348

349 *3.5. Macrobenthic diversity and abundance*

350 The detritus site had a biomass of accumulated macrophyte (*F. vesiculosus*) detritus of 1666 ± 223
351 g dry weight m⁻² (mean ± SE, n = 4), approximately 1.5-fold larger than nearby intact *F. vesiculosus*
352 canopies (Table 2). Detritus accumulation in the five other habitats was around 100-fold smaller.
353 The area of the detritus site estimated using Google Earth was 2300 m², amounting to 3,800.32 kg
354 dry weight of *F. vesiculosus* fragments. Macrofauna abundance ranged from 27,190 ± 9,008.54 ind.
355 m⁻² at the bare sediments site to 17,300.259 ± 24,002.4 ind. m⁻² at the sheltered *F. vesiculosus* site
356 (mean ± SE, n = 4) (Table 3). Macrofauna biomass ranged from 6 ± 2 g m⁻² at the bare site to 41 ± 9
357 g m⁻² at the exposed seagrass site (mean ± SE, n = 4), and the number of species ranged from 6 to
358 23, with the lowest values measured at the bare sediments and detritus sites, and the highest values
359 at the sheltered *F. vesiculosus* site (Table 3).

360 At the detritus site, there was a low abundance of epifaunal crustaceans when compared to other
361 habitats with canopies. Key species, such as the amphipod *Gammarus* spp. were notably absent, and
362 isopods such as *Idotea* spp. were present in low abundance (Table A34). Similarly, there was a
363 notable absence of bivalves such as the soft-shelled clam, *Mya arenaria*, and the cockle
364 *Cerastoderma glaucum*. Polychaetes such as *Hediste diversicolor* and *Marenzelleria* spp. were also

365 absent from the detritus site but present in other sedimentary habitats (Table A34). The nMDS
366 ordination of the macrofaunal assemblages indicated a clear separation of points representing the
367 different habitat sites (ANOSIM: $R^2 = 0.865$; $p < 0.001$). The assemblages from the bare sand and
368 the detritus sites formed separated site groupings compared to the vegetated sites ('*Fucus*' and
369 'seagrass', both exposed and sheltered). Within the vegetated sites, the assemblages of the 'seagrass
370 sheltered' and the '*Fucus* sheltered' sites were the most different (Fig. 72).

371

372 Table 2: Vegetation abundance and biomass (dry weight) at the six study sites. Abundance is shoots
 373 per m² for seagrass and individuals per m² for *F. vesiculosus*. Values are mean \pm SE.

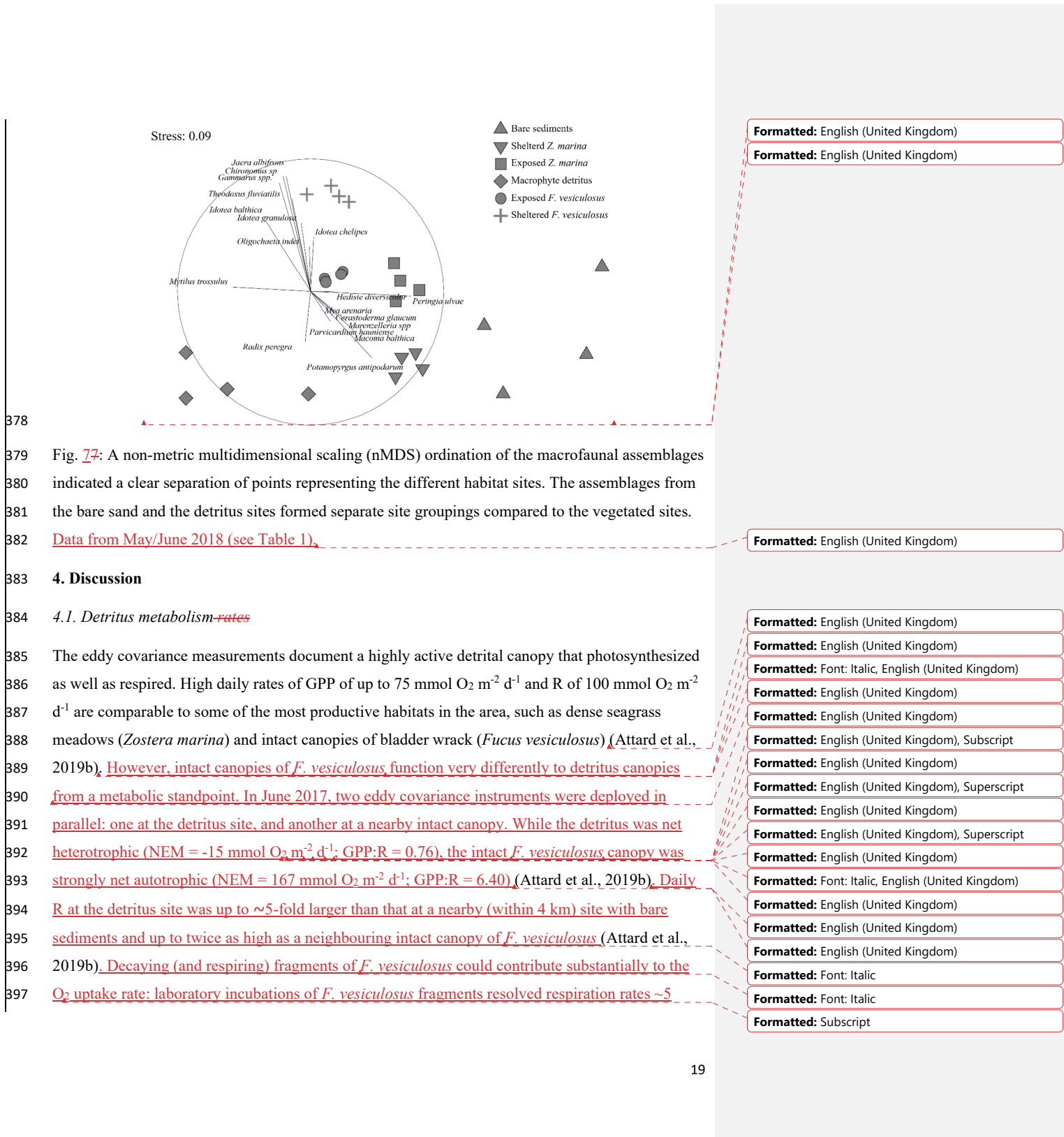
Site	Abundance per m ²	Above-ground biomass (g m ⁻²)	Belowground biomass (g m ⁻²)	Detritus (g m ⁻²)	Biomass other species (g m ⁻²)
Macrophyte detritus				1666 \pm 223	
Bare sediments					
Sheltered <i>Z. marina</i>	768 \pm 92	21 \pm 2	8 \pm 1	58 \pm 13	0.1 \pm 0.1
Exposed <i>Z. marina</i>	2565 \pm 164	69 \pm 7	25 \pm 3	16 \pm 2	0.2 \pm 0.2
Sheltered <i>F. vesiculosus</i>	16 \pm 2	1244 \pm 58		55 \pm 11	
Exposed <i>F. vesiculosus</i>	16 \pm 2	1112 \pm 119		20 \pm 2	

Formatted: English (United Kingdom)

374
 375 Table 3: Macrofauna abundance, biomass (ash-free dry weight), and number of species at the six
 376 study sites.

Site	Infrafauna abundance (ind. m ⁻²)	Epifauna abundance (ind. m ⁻²)	Total abundance (ind. m ⁻²)	Infrafauna biomass (g m ⁻²)	Epifauna biomass (g m ⁻²)	Total biomass (g m ⁻²)	Number of species
Macrophyte detritus	4175 \pm 2885	493 \pm 37	4668 \pm 2885	5 \pm 3	5 \pm 0	9 \pm 3	6
Bare sediments	2719 \pm 854	-	2719 \pm 854	6 \pm 2	-	6 \pm 2	6
Sheltered <i>Z. marina</i>	6110 \pm 787	3020 \pm 874	9130 \pm 1176	30 \pm 6	2 \pm 0	33 \pm 6	18
Exposed <i>Z. marina</i>	6959 \pm 620	3316 \pm 772	10275 \pm 990	31 \pm 8	10 \pm 2	41 \pm 9	16
Sheltered <i>F. vesiculosus</i>	-	17259 \pm 2421	17259 \pm 2421	-	11 \pm 2	11 \pm 2	23
Exposed <i>F. vesiculosus</i>	-	3551 \pm 609	3551 \pm 609	-	7 \pm 2	7 \pm 2	12

Formatted: English (United Kingdom)



398 $\mu\text{mol O}_2 \text{ g} \text{ dw}^{-1} \text{ h}^{-1}$, equivalent to $\sim 25 \text{ mmol O}_2 \text{ m}^{-2} \text{ d}^{-1}$ when upscaled to *in situ* biomass observed at
399 the detritus site (data not shown).

Formatted: Font: Italic

400 Notwithstanding the key metabolic differences between detritus and other neighbouring sites, the
401 flux measurements (Figure 4) These results indicate that shallow detritus accumulation zones are
402 not just regions of organic matter remineralization, but rather they synthesize substantial amounts of
403 organic matter through primary production. The range in daily GPP:R from 0.53 to 0.81 indicates
404 that primary production can offset a substantial proportion of the respiratory demand, which extends
405 the persistence of detritus in the coastal zone. These observations are consistent with the laboratory
406 study by Frontier et al. (2021), who determined that following detachment, kelp (*Laminaria*
407 *hyperborea* *hyperborea* and *L. ochroleuca*) fragments retain physiological and reproductive
408 capabilities for up to several months. Carbon retention within the coastal zone and export to deeper,
409 sedimentary accumulation regions would therefore be larger than would be predicted by
410 decomposition theory alone. Similarly, slow, and incomplete degradation of algae detritus under
411 low $[\text{O}_2]$ -conditions, which could occur, for instance, in the bottom layers of detrital canopies or in
412 the large anoxic basins of the Baltic Sea (Conley et al., 2009), would increase carbon retention,
413 transfer, and sequestration potential (Pedersen et al., 2021).

Formatted: English (United Kingdom)

Formatted: English (United Kingdom)

Formatted: English (United Kingdom)

414 4.2. *Hidden Periodic* benthic hypoxia

415 Our *in situ* measurements performed over a few days in late spring document that subtidal detritus
416 accumulation zones uniquely experience dynamic $[\text{O}_2]$ -conditions driven by sunlight availability
417 and flow velocity, with rapid $[\text{O}_2]$ -oscillations and frequent periods of hypoxia (Table 1). Hypoxic
418 conditions were largely restricted to the lower ~ 5 cm of the canopy and were only revealed by
419 sensors placed directly above the sediment surface (< 5 cm distance). At the onset of wave-driven
420 mixing, hypoxic waters from within the canopy propagated upwards into the water column and
421 were registered by fast-response $[\text{O}_2]$ -sensors located 10 cm above the canopy (~ 35 cm above the
422 seafloor). This observation suggests that the $[\text{O}_2]$ -conditions inside the entire canopy and even in
423 the water column directly above can reach hypoxic conditions for a few minutes (Fig. 34). Such
424 pulses, however, were not registered by the slow-response $[\text{O}_2]$ -optodes with a factory-specified T_{90}
425 < 2 min. The minimum $[\text{O}_2]$ -concentration observed by these sensors placed at 10 cm and 35 cm
426 above the seafloor was 158 and $229 \mu\text{mol L}^{-1}$, respectively, and thus well above hypoxic conditions.

Formatted: English (United Kingdom)

429 map spatial gradients in O_2 at < 5 cm distance to the seabed. Since and since then, other researchers
430 have investigated the distribution of dissolved constituents such as O_2 and nutrients in the benthic
431 boundary layer using motor driven sliders that transport sensors vertically towards the seafloor
432 (Holtappels et al., 2011). These studies document that solute gradients are largest near the seafloor
433 because the seafloor is a strong solute sink or source, and turbulent diffusivities are low. For
434 practical reasons, however, coastal monitoring programs measure $[O_2]$ further away from the
435 seafloor. Models based on monitoring data suggest that hypoxia is prevalent in only small areas of
436 the shallow subtidal zone. For instance, models for the northern Baltic Sea, which cover a total
437 seabed area of 12435 km^2 , of which 2211 km^2 is in shallow waters $< 5 \text{ m}$ depth, indicate that just
438 16.5 km^2 (or 0.75% of shallow waters) are prone to hypoxia (Virtanen et al., 2019). Given that large
439 quantities of drifting macrophytes are a common phenomenon in the shallow subtidal zone of the
440 northern Baltic Sea (Norkko and Bonsdorff, 1996a). It is therefore likely that coastal hypoxia in
441 the coastal zone is currently underestimated because large-scale models are largely based on
442 measurements performed higher above the seafloor (0.5–1.0 m) (Virtanen et al., 2019; Conley et al.,
443 2011).

Formatted: English (United Kingdom)

444 4.3. Biodiversity and $[O_2]$ oxygen dynamics in detritus canopies

445 Despite being considered a temporary habitat, detritus was found in abundance at our study site on
446 all occasions in May, June, and September. This type of habitat is likely quite widespread in the
447 Baltic. Habitat distribution models for the area indicate a dominance of *F. vesiculosus* canopies in
448 shallow waters $< 5 \text{ m}$ depth (Virtanen et al., 2018), and these canopies are expected to export
449 substantial amounts of organic matter ($\sim 0.3 \text{ kg C m}^{-2} \text{ yr}^{-1}$) (Attard et al., 2019a) which can
450 accumulate in topographical depressions with limited water exchange (Attard et al., 2019a).
451 Topographical depressions occupy $\sim 1350 \text{ km}^2$ or $\sim 11\%$ of the northern Baltic Sea (Virtanen et al.,
452 2019). During a recent seasonal study, we observed the highest abundance of detritus at our study
453 site in summer and autumn, coinciding with high southerly winds that erode intact canopies in
454 shallower waters (Attard et al., 2019a). However, we also observed significant canopy erosion in
455 winter when a substantial biomass of *F. vesiculosus* froze into sea ice and got dislodged once the ice
456 broke up (Fig. 78). Therefore, some degree of drifting detritus might be common throughout the
457 year. Drifting detritus constitutes a significant habitat structure. Given high enough biomass,
458 however, detritus canopies can be a challenging habitat for most species. Dense canopies induce
459 drag, suppress local turbulence, and curb the exchange of O_2 and other nutrients between the
460 benthic boundary layer and the seafloor (Hansen and Reidenbach, 2017). If O_2 -consumption within

Formatted: English (United Kingdom)

Formatted: English (United Kingdom)

Formatted: English (United Kingdom)

Formatted: English (United Kingdom), Superscript

Formatted: English (United Kingdom)

Formatted: English (United Kingdom), Superscript

Formatted: English (United Kingdom)

Formatted: English (United Kingdom), Superscript

Formatted: English (United Kingdom)

Formatted: English (United Kingdom), Superscript

Formatted: English (United Kingdom)

Formatted: Font: (Default) Times New Roman, English (United Kingdom)

Formatted: English (United Kingdom)

Formatted: English (United Kingdom), Superscript

Formatted: English (United Kingdom)

Formatted: English (United Kingdom), Superscript

Formatted: English (United Kingdom)

461 the canopy and underlying sediments exceeds O₂ supply from the water column, low O₂ conditions
462 develop, resulting in hotspots of anoxia and hydrogen sulfide production, inducing mortality of
463 sedentary species (Norkko and Bonsdorff, 1996a; Glud et al., 2004; Norkko et al., 2013). At our
464 study site, hypoxic conditions uniquely occurred at the detritus site and for around a quarter of the
465 deployment time (Table 1). We can expect these conditions to be particularly challenging for
466 crustaceans, the most hypoxia-sensitive macroinvertebrate group (Vaquer-Sunyer and Duarte,
467 2008). Indeed, we only found one crustacean species at this site- the isopod *Idotea balthica* (Table
468 A+3)- which is mobile and can tolerate hypoxic conditions for a few hours (Vetter and Dayton,
469 1999). All other invertebrates observed at the detritus site were mollusks (Table A34), the most
470 hypoxia-tolerant marine invertebrate group (Vaquer-Sunyer and Duarte, 2008). Other tolerant
471 species include the blue mussel *Mytilus trossulus x edulis* that can survive > 300 h of anoxia
472 (Jorgensen, 1980), although the survival of larvae depends on its developmental stage (Diaz and
473 Rosenberg, 1995). Similarly, the mudsnail *Peringia ulvae* is highly mobile and can survive > 150 h
474 of anoxia (Jorgensen, 1980; Norkko et al., 2000).

475 Overall, the dynamic [O₂] conditions in detrital canopies seem to be challenging for most species in
476 this region of the Baltic Sea, with lethal and non-lethal thresholds frequently being exceeded on
477 timescales of hours to days. We currently have a poor understanding of the extent of
478 'hidden' periodic hypoxia in coastal waters, because [O₂] measurements are performed at some
479 distance away from the seabed. While this is a practical approach that is done to minimize sensor
480 fouling and damage, it does not reveal the full extent of coastal hypoxia. If implemented widely,
481 sensor arrays, as described herein, and sensor elevators (e.g. (Holtappels et al., 2011)) can fill in this
482 knowledge gap and provide important insights into the ecological status and biogeochemical
483 cycling that is needed for the sustainable management of coastal ecosystems.



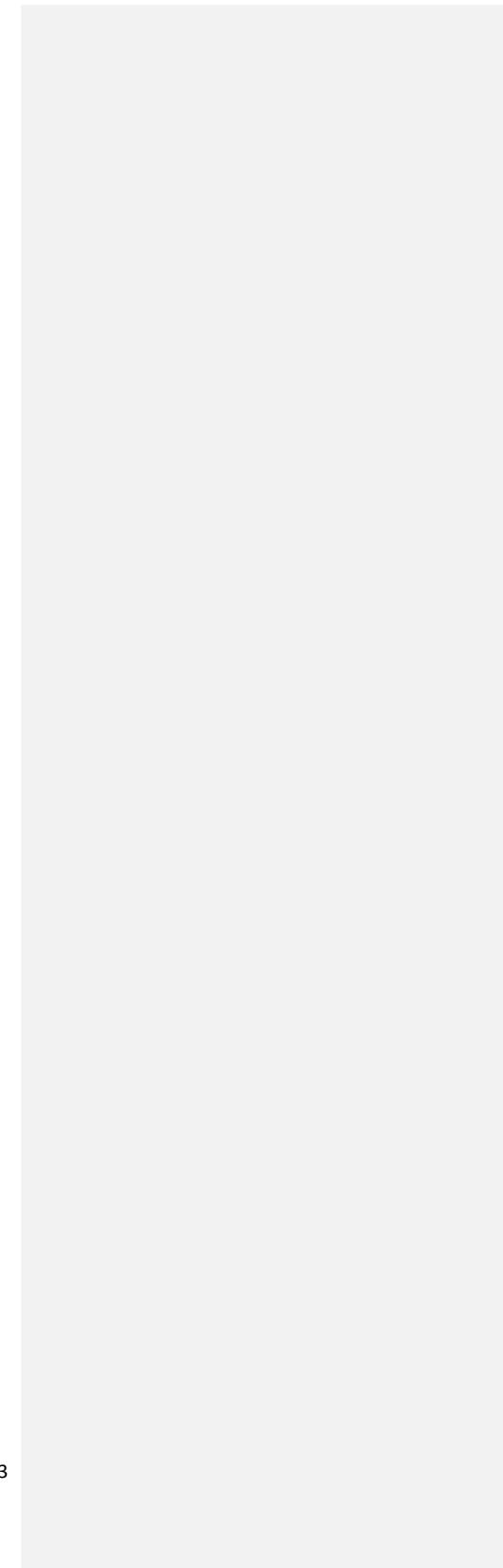
484

Formatted: English (United Kingdom)
Formatted: English (United Kingdom)

Formatted: English (United Kingdom)
Formatted: English (United Kingdom)

Formatted: English (United Kingdom)
Formatted: English (United Kingdom)

485 Fig. 88: substantial detritus accumulation was observed in late winter (March 2021) when *F.*
486 *vesiculosus* froze into sea ice and got dislodged once the ice broke up. (Photo by Alf Norkko)



487 Table A1: A summary of the eddy covariance flux measurements performed on the detritus canopy
488 during the three measurement campaigns. Daily integrated seabed PAR and detritus light-use
489 efficiency (LUE, calculated as daily GPP/daily PAR) are also presented.

<u>Field campaign</u>	<u>Day</u>	<u>Daily GPP (mmol O₂ m⁻² d⁻¹)</u>	<u>Daily R (mmol O₂ m⁻² d⁻¹)</u>	<u>GPP:R</u>	<u>Daily PAR (mmol photons m⁻² d⁻¹)</u>	<u>LUE (O₂ photon⁻¹)</u>
Jun 2017	1	62	83	0.74	13554	0.005
	2	54	71	0.76	11710	0.005
	3	29	35	0.81	9044	0.003
Sep 2017	1	15	26	0.57	3013	0.005
	2	37	69	0.54	4827	0.008
	3	26	48	0.53	3815	0.007
May 2018	1	46	59	0.77	10997	0.004
	2	57	74	0.76	12732	0.004
	3	74	97	0.76	13336	0.006
	4	32	41	0.78	10523	0.003
	5	39	51	0.77	10915	0.004

Formatted Table

Formatted: Font: (Default) Times New Roman, 12 pt, Not Bold, English (United Kingdom)

Formatted: Font: (Default) Times New Roman, 12 pt, English (United Kingdom)

Formatted: Font: (Default) Times New Roman, 12 pt, English (United Kingdom)

Formatted: Font: (Default) Times New Roman, 12 pt, English (United Kingdom)

Formatted: ... [10]

Formatted: ... [11]

Formatted: ... [9]

Formatted: ... [13]

Formatted: ... [14]

Formatted: ... [12]

Formatted: ... [15]

Formatted: ... [16]

Formatted: ... [17]

Formatted: ... [19]

Formatted: ... [20]

Formatted: ... [18]

Formatted: ... [22]

Formatted: ... [23]

Formatted: ... [21]

Formatted: ... [24]

Formatted: ... [25]

Formatted: ... [26]

Formatted: ... [28]

Formatted: ... [29]

Formatted: ... [27]

Formatted: ... [31]

Formatted: ... [32]

Formatted: ... [30]

Formatted: ... [34]

Formatted: ... [35]

Formatted: ... [37]

Formatted: ... [38]

Formatted: ... [36]

Formatted: English (United Kingdom)

492 **Table A2:** Fit statistics for linear regressions performed between daily detritus GPP and R, and daily
 493 GPP and benthic PAR. Where relevant, values are presented \pm SE. The SE was scaled with the
 494 square root of the reduced Chi-Sqr. ANOVA was used to test slope significance. Asterisks indicate
 495 that the slope was significantly different from zero at the 0.05 level.

Relationship between daily GPP and daily R				
Field campaign	Slope of linear regression \pm SE	Intercept \pm SE	R^2	ANOVA
				Prob $>$ F
Jun 2017	1.43 \pm 0.02	-5.91 \pm 0.77	0.99	0.01*
Sep 2017	1.93 \pm 0.06	-2.19 \pm 1.70	0.99	0.02*
May 2018	1.33 \pm 0.00	-1.09 \pm 0.17	0.99	0.00*
Global	1.16 \pm 0.13	9.90 \pm 5.92	0.89	0.00*

Relationship between daily GPP and daily PAR				
Field campaign	Slope of linear regression \pm SE	Intercept \pm SE	R^2	ANOVA
				Prob $>$ F
Jun 2017	128 \pm 23	5293 \pm 1164	0.94	0.11
Sep 2017	82 \pm 4	1765 \pm 121	0.99	0.03*
May 2018	73 \pm 12	8103 \pm 609	0.90	0.01*
Global	182 \pm 40	1725 \pm 1852	0.66	0.00*

Formatted	[39]
Formatted	[40]
Formatted	[41]
Formatted Table	[42]
Formatted	[43]
Formatted	[46]
Formatted	[47]
Formatted	[44]
Formatted	[45]
Formatted	[48]
Formatted	[49]
Formatted	[51]
Formatted	[52]
Formatted	[53]
Formatted	[54]
Formatted	[50]
Formatted	[55]
Formatted	[57]
Formatted	[58]
Formatted	[59]
Formatted	[60]
Formatted	[56]
Formatted	[61]
Formatted	[63]
Formatted	[64]
Formatted	[65]
Formatted	[66]
Formatted	[62]
Formatted	[67]
Formatted	[68]
Formatted	[69]
Formatted	[70]
Formatted	[71]
Formatted	[72]
Formatted	[73]
Formatted	[74]
Formatted	[75]
Formatted	[76]
Formatted	[79]
Formatted	[80]
Formatted	[77]
Formatted	[78]
Formatted	[81]
Formatted	[82]
Formatted	[84]
Formatted	[85]
Formatted	[83]
Formatted	[86]
Formatted	[88]
Formatted	[89]
Formatted	[87]
Formatted	[90]
Formatted	[92]
Formatted	[93]
Formatted	[91]
Formatted	[94]
Formatted	[96]

Table A34: Species list for the five studied sites. Presence is indicated by 'x'.

Group	Species	Macrophyt e detritus	Bare sediment s	Sheltered Z. marina	Exposed Z. marina	Sheltered F. vesiculosu s	Exposed F. vesiculosu s
Crustacea	<i>Amphibalan us improvisus</i>			x			
	<i>Asellus aquaticus</i>					x	
	<i>Corophium spp.</i>			x			
	<i>Gammarus spp.</i>			x	x	x	x
	<i>Idotea balthica</i>	x			x	x	x
	<i>Idotea chelipes</i>				x	x	x
	<i>Idotea granulosa</i>			x	x	x	x
	<i>Jaera albifrons</i>			x	x	x	x
	Cladocera					x	
	Copepoda					x	
	Ostracoda sp.					x	
	Mysid					x	x
Bivalvia	<i>Cerastoderma glaucum</i>			x	x		
	<i>Parvicardium hauniense</i>			x	x		
	<i>Macoma balthica</i>	x	x	x	x	x	x
	<i>Mya arenaria</i>			x	x		
	<i>Mytilus trossulus x edulis</i>	x		x	x	x	x
Gastropoda	<i>Peringia ulvae</i>	x	x	x	x	x	x
	<i>Radix</i> sp.	x		x			x
	<i>Potamopyrgus antipodarum</i>		x	x			
	<i>Theodoxus fluviatilis</i>	x	x	x	x	x	x

Formatted: English (United Kingdom)

Polychaeta	<i>Hediste diversicolor</i>			X	X		
	<i>Halicryptus spinulosus</i>					X	
	<i>Maranzelleria spp.</i>		X	X	X	X	
	Nematoda					X	
	Oligochaeta			X	X	X	
	<i>Pygospio elegans</i>					X	
Others	<i>Chironomus sp</i>			X	X	X	X
	Coleoptera larvae						X
	Odonata						X
	<i>Cyanophthalma obscura</i>						X
	Hydrachnidae		X				X

Formatted: English (United Kingdom)

500 **Author contribution**

501 All authors contributed significantly to designing the research, funding the study, collecting the
502 data, analyzing samples and data, and interpreting the results. KMA wrote the paper with input from
503 all authors.

504 **Competing interests**

505 The authors declare that they have no conflict of interest

506 **Data availability**

507 All data presented in this paper will be made available in a FAIR-aligned data repository upon
508 acceptance of the paper.

509 **Acknowledgements**

510 Colleagues at the Tvärminne Zoological Station provided help with fieldwork and logistics. Anni
511 Glud at the University of Southern Denmark constructed the oxygen microsensors used in this
512 study. Elina Virtanen at the Finnish Environmental Institute (SYKE) provided spatial data used to
513 estimate the potential extent of detritus canopies. The Walter and Andrée de Nottbeck Foundation
514 supported this work through a postdoctoral fellowship to KMA and through a Masters fellowship to
515 AL. Further funding for this project was provided by research grants from the Academy of Finland
516 (project ID 294853), the University of Helsinki and Stockholm University strategic fund for
517 collaborative research (the Baltic Bridge initiative), and Denmark's Independent Research Fund
518 (project ID 7014-00078). This study has utilized research infrastructure facilities provided by
519 FINMARI (Finnish Marine Research Infrastructure network, The Academy of Finland, project ID
520 283417).

521 **References**

522 Attard, K. M. and Glud, R. N.: Technical Note: Estimating light-use efficiency of benthic habitats using
523 underwater O-2 eddy covariance, *Biogeosciences*, 17, 4343-4353, 2020.

524 Attard, K. M., Rodil, I. F., Berg, P., Norkko, J., Norkko, A., and Glud, R. N.: Seasonal metabolism and carbon
525 export potential of a key coastal habitat: The perennial canopy-forming macroalga *Fucus vesiculosus*,
526 *Limnol Oceanogr*, 64, 149-164, 10.1002/lo.11026, 2019a.

527 Attard, K. M., Rodil, I. F., Glud, R. N., Berg, P., Norkko, J., and Norkko, A.: Seasonal ecosystem metabolism
528 across shallow benthic habitats measured by aquatic eddy covariance, *Limnology and Oceanography
529 Letters*, 4, 79-86, 10.1002/lo.10107, 2019b.

530 Berg, P. and Pace, M. L.: Continuous measurement of air-water gas exchange by underwater eddy
531 covariance, *Biogeosciences*, 14, 5595-5606, 2017.

532 Berg, P., Røy, H., and Wiberg, P. L.: Eddy correlation flux measurements: the sediment surface area that
533 contributes to the flux, *Limnol Oceanogr*, 52, 1672-1684, 10.4319/lo.2007.52.4.1672, 2007.

534 Berg, P., Huettel, M., Glud, R. N., Reimers, C. E., and Attard, K. M.: Aquatic Eddy Covariance: The Method
535 and Its Contributions to Defining Oxygen and Carbon Fluxes in Marine Environments, *Annual Review of
536 Marine Science*, 14, 431-455, 10.1146/annurev-marine-042121-012329, 2022.

537 Berg, P., Røy, H., Janssen, F., Meyer, V., Jorgensen, B. B., Huettel, M., and de Beer, D.: Oxygen uptake by
538 aquatic sediments measured with a novel non-invasive eddy-correlation technique, *Marine Ecology
539 Progress Series*, 261, 75-83, 10.3354/Meps261075, 2003.

540 Bittig, H. C., Kortzinger, A., Neill, C., van Ooijen, E., Plant, J. N., Hahn, J., Johnson, K. S., Yang, B., and
541 Emerson, S. R.: Oxygen Optode Sensors: Principle, Characterization, Calibration, and Application in the
542 Ocean, *Frontiers in Marine Science*, 4, 2018.

543 Breitburg, D., Levin, L. A., Oschlies, A., Gregoire, M., Chavez, F. P., Conley, D. J., Garcon, V., Gilbert, D.,
544 Gutierrez, D., Isensee, K., Jacinto, G. S., Limburg, K. E., Montes, I., Naqvi, S. W. A., Pitcher, G. C., Rabalais, N.,
545 Roman, M. R., Rose, K. A., Seibel, B. A., Telszewski, M., Yasuhara, M., and Zhang, J.: Declining oxygen in
546 the global ocean and coastal waters, *Science*, 359, 46-+, 2018.

547 Broch, O. J., Hancke, K., and Ellingsen, I. H.: Dispersal and Deposition of Detritus From Kelp Cultivation,
548 *Frontiers in Marine Science*, 9, 2022.

549 Broch, O. J., Alver, M. O., Bekkby, T., Gundersen, H., Forbord, S., Handa, A., Skjermo, J., and Hancke, K.: The
550 Kelp Cultivation Potential in Coastal and Offshore Regions of Norway, *Frontiers in Marine Science*, 5, 2019.

551 Camillini, N., Attard, K. M., Eyre, B. D., and Glud, R. N.: Resolving community metabolism of eelgrass *Zostera
552 marina* meadows by benthic flume-chambers and eddy covariance in dynamic coastal environments,
553 *Marine Ecology Progress Series*, 661, 97-114, 2021.

554 Carstensen, J. and Conley, D. J.: Baltic Sea Hypoxia Takes Many Shapes and Sizes, *Limnology and
555 Oceanography Bulletin*, 28, 125-129, <https://doi.org/10.1002/lob.10350>, 2019.

556 Conley, D. J., Carstensen, J., Aigars, J., Axe, P., Bonsdorff, E., Eremina, T., Haahti, B. M., Humborg, C.,
557 Jonsson, P., Kotta, J., Lannegren, C., Larsson, U., Maximov, A., Medina, M. R., Lysiak-Pastuszak, E.,
558 Remeikaite-Nikiene, N., Walve, J., Wilhelms, S., and Zillen, L.: Hypoxia Is Increasing in the Coastal Zone of
559 the Baltic Sea, *Environ Sci Technol*, 45, 6777-6783, 10.1021/es201212r, 2011.

560 Conley, D. J., Bjorck, S., Bonsdorff, E., Carstensen, J., Destouni, G., Gustafsson, B. G., Hietanen, S.,
561 Kortekaas, M., Kuosa, H., Meier, H. E. M., Muller-Karulis, B., Nordberg, K., Norkko, A., Nurnberg, G.,
562 Pitkanen, H., Rabalais, N. N., Rosenberg, R., Savchuk, O. P., Slomp, C. P., Voss, M., Wulff, F., and Zillen, L.:
563 Hypoxia-Related Processes in the Baltic Sea, *Environ Sci Technol*, 43, 3412-3420, 10.1021/es802762a, 2009.

564 Davanzo, C. and Kremer, J. N.: Diel Oxygen Dynamics and Anoxic Events in an Eutrophic Estuary of Waquoit
565 Bay, Massachusetts, *Estuaries*, 17, 131-139, 1994.

566 Diaz, R. J. and Rosenberg, R.: Marine benthic hypoxia: A review of its ecological effects and the behavioural
567 responses of benthic macrofauna, *Oceanography and Marine Biology - an Annual Review*, Vol 33, 33, 245-
568 303, 1995.

569 Diaz, R. J. and Rosenberg, R.: Spreading dead zones and consequences for marine ecosystems, *Science*, 321,
570 926-929, 10.1126/science.1156401, 2008.

Formatted: English (United Kingdom)

Formatted: English (United Kingdom)

571 Duarte, C. M. and Cebrián, J.: The fate of marine autotrophic production, *Limnol Oceanogr*, 41, 1758-1766,
572 DOI 10.4319/lo.1996.41.8.1758, 1996.

573 Fenchel, T. and Glud, R. N.: Benthic primary production and O₂-CO₂ dynamics in a shallow-water sediment:
574 Spatial and temporal heterogeneity, *Ophelia*, 53, 159-171, 2000.

575 Frontier, N., de Bettignies, F., Foggo, A., and Davout, D.: Sustained productivity and respiration of
576 degrading kelp detritus in the shallow benthos: Detached or broken, but not dead, *Mar Environ Res*, 166,
577 2021.

578 Garcia, H. E. and Gordon, L. I.: Oxygen Solubility in Seawater - Better Fitting Equations, *Limnol Oceanogr*,
579 37, 1307-1312, 1992.

580 Glud, R. N.: Oxygen dynamics of marine sediments, *Mar Biol Res*, 4, 243-289, 2008.

581 Glud, R. N., Rysgaard, S., Fenchel, T., and Nielsen, P. H.: A conspicuous H₂S-oxidizing microbial mat from a
582 high-latitude Arctic fjord (Young Sound, NE Greenland), *Mar Biol*, 145, 51-60, DOI 10.1007/s00227-004-
583 1296-8, 2004.

584 Holtappels, M., Kuypers, M. M. M., Schluter, M., and Bruchert, V.: Measurement and interpretation of
585 solute concentration gradients in the benthic boundary layer, *Limnol Oceanogr-Meth*, 9, 1-13, 2011.

586 Jorgensen, B. B.: Seasonal Oxygen Depletion in the Bottom Waters of a Danish Fjord and Its Effect on the
587 Benthic Community, *Oikos*, 34, 68-76, 1980.

588 Juska, I. and Berg, P.: Variation in seagrass meadow respiration measured by aquatic eddy covariance,
589 *Limnology and Oceanography Letters*, 7, 410-418, <https://doi.org/10.1002/lo2.10276>, 2022.

590 Krumhansl, K. A. and Scheibling, R. E.: Production and fate of kelp detritus, *Marine Ecology Progress Series*,
591 467, 281-302, 10.3354/meps09940, 2012.

592 Long, M. H. and Nicholson, D. P.: Surface gas exchange determined from an aquatic eddy covariance
593 floating platform, *Limnol Oceanogr-Meth*, 16, 145-159, 2018.

594 McGinnis, D. F., Cherednichenko, S., Sommer, S., Berg, P., Rovelli, L., Schwarz, R., Glud, R. N., and Linke, P.:
595 Simple, robust eddy correlation amplifier for aquatic dissolved oxygen and hydrogen sulfide flux
596 measurements, *Limnol Oceanogr-Meth*, 9, 340-347, DOI 10.4319/lom.2011.9.340, 2011.

597 Middelburg, J. J. and Levin, L. A.: Coastal hypoxia and sediment biogeochemistry, *Biogeosciences*, 6, 1273-
598 1293, DOI 10.5194/bg-6-1273-2009, 2009.

599 Norkko, A. and Bonsdorff, E.: Population responses of coastal zoobenthos to stress induced by drifting algal
600 mats, *Marine Ecology Progress Series*, 140, 141-151, DOI 10.3354/meps140141, 1996a.

601 Norkko, A. and Bonsdorff, E.: Rapid zoobenthic community responses to accumulations of drifting algae,
602 *Marine Ecology Progress Series*, 131, 143-157, DOI 10.3354/meps131143, 1996b.

603 Norkko, J., Bonsdorff, E., and Norkko, A.: Drifting algal mats as an alternative habitat for benthic
604 invertebrates: Species specific responses to a transient resource, *Journal of Experimental Marine Biology
and Ecology*, 248, 79-104, 2000.

605 Pedersen, M. F., Filbee-Dexter, K., Frisk, N. L., Sarossy, Z., and Wernberg, T.: Carbon sequestration potential
606 increased by incomplete anaerobic decomposition of kelp detritus, *Marine Ecology Progress Series*, 660, 53-
607 67, 2021.

608 Platt, T., Gallegos, C. L., and Harrison, W. G.: Photoinhibition of photosynthesis in natural assemblages of
609 marine phytoplankton, *J Mar Res*, 38, 687-701, 1980.

610 Rheuban, J. E., Berg, P., and McGlathery, K. J.: Multiple timescale processes drive ecosystem metabolism in
611 eelgrass (*Zostera marina*) meadows, *Marine Ecology Progress Series*, 507, 1-13, 10.3354/meps10843, 2014.

612 Robertson, E. K., Roberts, K. L., Burdorf, L. D. W., Cook, P., and Thamdrup, B.: Dissimilatory nitrate reduction
613 to ammonium coupled to Fe(II) oxidation in sediments of a periodically hypoxic estuary, *Limnol Oceanogr*,
614 61, 365-381, 2016.

615 Rodil, I. F., Attard, K. M., Norkko, J., Glud, R. N., and Norkko, A.: Towards a sampling design for
616 characterizing habitat-specific benthic biodiversity related to oxygen flux dynamics using Aquatic Eddy
617 Covariance, *Plos One*, 14, e0211673, 10.1371/journal.pone.0211673, 2019.

618 Rumohr, H., Brey, T., and Ankar, S.: A compilation of biometric conversion factors for benthic invertebrates
619 of the Baltic Sea, *Baltic Marine Biologists*, 9, 1-56, 1987.

620

621 Smith, S. V.: Marine macrophytes as a global carbon sink, *Science*, 211, 838-840, DOI
622 10.1126/science.211.4484.838, 1981.

623 Tyler, R. M., Brady, D. C., and Targett, T. E.: Temporal and Spatial Dynamics of Diel-Cycling Hypoxia in
624 Estuarine Tributaries, *Estuar Coast*, 32, 123-145, 10.1007/s12237-008-9108-x, 2009.

625 Vaquer-Sunyer, R. and Duarte, C. M.: Thresholds of hypoxia for marine biodiversity, *P Natl Acad Sci USA*,
626 105, 15452-15457, 10.1073/pnas.0803833105, 2008.

627 Vetter, E. W. and Dayton, P. K.: Organic enrichment by macrophyte detritus, and abundance patterns of
628 megafaunal populations in submarine canyons, *Marine Ecology Progress Series*, 186, 137-148, 1999.

629 Virtanen, E., Viitasalo, M., Lappalainen, J., and Moilanen, A.: Evaluation, gap analysis, and potential
630 expansion of the Finnish marine protected area network, *Frontiers in Marine Science*,
631 10.3389/fmars.2018.00402, 2018.

632 Virtanen, E. A., Norkko, A., Sandman, A. N., and Viitasalo, M.: Identifying areas prone to coastal hypoxia -
633 the role of topography, *Biogeosciences*, 16, 3183-3195, 2019.

634

Formatted: English (United Kingdom)

Page 7: [1] Formatted	Karl Michael Attard	10-01-2023 11:08:00
English (United Kingdom)		◀
▲		
Page 7: [1] Formatted	Karl Michael Attard	10-01-2023 11:08:00
English (United Kingdom)		◀
▲		
Page 7: [1] Formatted	Karl Michael Attard	10-01-2023 11:08:00
English (United Kingdom)		◀
▲		
Page 7: [1] Formatted	Karl Michael Attard	10-01-2023 11:08:00
English (United Kingdom)		◀
▲		
Page 7: [1] Formatted	Karl Michael Attard	10-01-2023 11:08:00
English (United Kingdom)		◀
▲		
Page 7: [1] Formatted	Karl Michael Attard	10-01-2023 11:08:00
English (United Kingdom)		◀
▲		
Page 7: [1] Formatted	Karl Michael Attard	10-01-2023 11:08:00
English (United Kingdom)		◀
▲		
Page 7: [1] Formatted	Karl Michael Attard	10-01-2023 11:08:00
English (United Kingdom)		◀
▲		
Page 7: [1] Formatted	Karl Michael Attard	10-01-2023 11:08:00
English (United Kingdom)		◀
▲		
Page 7: [2] Formatted	Karl Michael Attard	10-01-2023 11:08:00
English (United Kingdom)		◀
▲		
Page 7: [2] Formatted	Karl Michael Attard	10-01-2023 11:08:00
English (United Kingdom)		◀
▲		
Page 7: [3] Formatted	Karl Michael Attard	10-01-2023 11:08:00
English (United Kingdom)		◀
▲		
Page 7: [3] Formatted	Karl Michael Attard	10-01-2023 11:08:00
English (United Kingdom)		◀
▲		

Page 7: [6] Formatted Karl Michael Attard 14-01-2023 17:35:00

Subscript

Page 7: [6] Formatted Karl Michael Attard 14-01-2023 17:35:00

Subscript

Page 7: [6] Formatted Karl Michael Attard 14-01-2023 17:35:00

Subscript

Page 7: [6] Formatted Karl Michael Attard 14-01-2023 17:35:00

Subscript

Page 7: [6] Formatted Karl Michael Attard 14-01-2023 17:35:00

Subscript

Page 7: [6] Formatted Karl Michael Attard 14-01-2023 17:35:00

Subscript

Page 7: [6] Formatted Karl Michael Attard 14-01-2023 17:35:00

Subscript

Page 7: [6] Formatted Karl Michael Attard 14-01-2023 17:35:00

Subscript

Page 7: [6] Formatted Karl Michael Attard 14-01-2023 17:35:00

Subscript

Page 7: [6] Formatted Karl Michael Attard 14-01-2023 17:35:00

Subscript

Page 7: [6] Formatted Karl Michael Attard 14-01-2023 17:35:00

Subscript

Page 7: [6] Formatted Karl Michael Attard 14-01-2023 17:35:00

Subscript

Page 7: [6] Formatted Karl Michael Attard 14-01-2023 17:35:00

Subscript

Page 7: [6] Formatted Karl Michael Attard 14-01-2023 17:35:00

Subscript

Page 7: [6] Formatted Karl Michael Attard 14-01-2023 17:35:00

Subscript

Page 7: [6] Formatted	Karl Michael Attard	14-01-2023 17:35:00
Subscript		
▲		
Page 7: [6] Formatted	Karl Michael Attard	14-01-2023 17:35:00
Subscript		
▲		
Page 7: [6] Formatted	Karl Michael Attard	14-01-2023 17:35:00
Subscript		
▲		
Page 7: [6] Formatted	Karl Michael Attard	14-01-2023 17:35:00
Subscript		
▲		
Page 7: [7] Formatted	Karl Michael Attard	10-01-2023 11:08:00
English (United Kingdom)		
▲		
Page 7: [7] Formatted	Karl Michael Attard	10-01-2023 11:08:00
English (United Kingdom)		
▲		
Page 7: [7] Formatted	Karl Michael Attard	10-01-2023 11:08:00
English (United Kingdom)		
▲		
Page 7: [7] Formatted	Karl Michael Attard	10-01-2023 11:08:00
English (United Kingdom)		
▲		
Page 7: [7] Formatted	Karl Michael Attard	10-01-2023 11:08:00
English (United Kingdom)		
▲		
Page 7: [7] Formatted	Karl Michael Attard	10-01-2023 11:08:00
English (United Kingdom)		
▲		
Page 7: [7] Formatted	Karl Michael Attard	10-01-2023 11:08:00
English (United Kingdom)		
▲		
Page 7: [7] Formatted	Karl Michael Attard	10-01-2023 11:08:00
English (United Kingdom)		
▲		
Page 7: [8] Formatted	Karl Michael Attard	10-01-2023 11:08:00
English (United Kingdom)		
▲		

Page 7: [8] Formatted	Karl Michael Attard	10-01-2023 11:08:00
English (United Kingdom)		
Page 7: [8] Formatted	Karl Michael Attard	10-01-2023 11:08:00
English (United Kingdom)		
Page 24: [9] Formatted	Karl Michael Attard	10-01-2023 11:08:00
Font: (Default) Times New Roman, 12 pt, English (United Kingdom)		
Page 24: [10] Formatted	Karl Michael Attard	10-01-2023 11:08:00
Font: (Default) Times New Roman, 12 pt, English (United Kingdom)		
Page 24: [11] Formatted	Karl Michael Attard	10-01-2023 11:08:00
Font: (Default) Times New Roman, 12 pt, English (United Kingdom)		
Page 24: [12] Formatted	Karl Michael Attard	10-01-2023 11:08:00
Font: (Default) Times New Roman, 12 pt, English (United Kingdom)		
Page 24: [13] Formatted	Karl Michael Attard	10-01-2023 11:08:00
Font: (Default) Times New Roman, 12 pt, English (United Kingdom)		
Page 24: [14] Formatted	Karl Michael Attard	10-01-2023 11:08:00
Font: (Default) Times New Roman, 12 pt, English (United Kingdom)		
Page 24: [15] Formatted	Karl Michael Attard	10-01-2023 11:08:00
Font: (Default) Times New Roman, 12 pt, English (United Kingdom)		
Page 24: [16] Formatted	Karl Michael Attard	10-01-2023 11:08:00
Font: (Default) Times New Roman, 12 pt, English (United Kingdom)		
Page 24: [17] Formatted	Karl Michael Attard	10-01-2023 11:08:00
Font: (Default) Times New Roman, 12 pt, English (United Kingdom)		
Page 24: [18] Formatted	Karl Michael Attard	10-01-2023 11:08:00
Font: (Default) Times New Roman, 12 pt, English (United Kingdom)		
Page 24: [19] Formatted	Karl Michael Attard	10-01-2023 11:08:00
Font: (Default) Times New Roman, 12 pt, English (United Kingdom)		
Page 24: [20] Formatted	Karl Michael Attard	10-01-2023 11:08:00
Font: (Default) Times New Roman, 12 pt, English (United Kingdom)		
Page 24: [21] Formatted	Karl Michael Attard	10-01-2023 11:08:00
Font: (Default) Times New Roman, 12 pt, English (United Kingdom)		

Page 24: [22] Formatted	Karl Michael Attard	10-01-2023 11:08:00
Font: (Default) Times New Roman, 12 pt, English (United Kingdom)		
Page 24: [23] Formatted	Karl Michael Attard	10-01-2023 11:08:00
Font: (Default) Times New Roman, 12 pt, English (United Kingdom)		
Page 24: [24] Formatted	Karl Michael Attard	10-01-2023 11:08:00
Font: (Default) Times New Roman, 12 pt, English (United Kingdom)		
Page 24: [25] Formatted	Karl Michael Attard	10-01-2023 11:08:00
Font: (Default) Times New Roman, 12 pt, English (United Kingdom)		
Page 24: [26] Formatted	Karl Michael Attard	10-01-2023 11:08:00
Font: (Default) Times New Roman, 12 pt, English (United Kingdom)		
Page 24: [27] Formatted	Karl Michael Attard	10-01-2023 11:08:00
Font: (Default) Times New Roman, 12 pt, English (United Kingdom)		
Page 24: [28] Formatted	Karl Michael Attard	10-01-2023 11:08:00
Font: (Default) Times New Roman, 12 pt, English (United Kingdom)		
Page 24: [29] Formatted	Karl Michael Attard	10-01-2023 11:08:00
Font: (Default) Times New Roman, 12 pt, English (United Kingdom)		
Page 24: [30] Formatted	Karl Michael Attard	10-01-2023 11:08:00
Font: (Default) Times New Roman, 12 pt, English (United Kingdom)		
Page 24: [31] Formatted	Karl Michael Attard	10-01-2023 11:08:00
Font: (Default) Times New Roman, 12 pt, English (United Kingdom)		
Page 24: [32] Formatted	Karl Michael Attard	10-01-2023 11:08:00
Font: (Default) Times New Roman, 12 pt, English (United Kingdom)		
Page 24: [33] Formatted	Karl Michael Attard	10-01-2023 11:08:00
Font: (Default) Times New Roman, 12 pt, English (United Kingdom)		
Page 24: [34] Formatted	Karl Michael Attard	10-01-2023 11:08:00
Font: (Default) Times New Roman, 12 pt, English (United Kingdom)		
Page 24: [35] Formatted	Karl Michael Attard	10-01-2023 11:08:00
Font: (Default) Times New Roman, 12 pt, English (United Kingdom)		
Page 24: [36] Formatted	Karl Michael Attard	10-01-2023 11:08:00
Font: (Default) Times New Roman, 12 pt, English (United Kingdom)		

Page 24: [37] Formatted Karl Michael Attard 10-01-2023 11:08:00

Font: (Default) Times New Roman, 12 pt, English (United Kingdom)

Page 24: [38] Formatted Karl Michael Attard 10-01-2023 11:08:00

Font: (Default) Times New Roman, 12 pt, English (United Kingdom)

Page 25: [39] Formatted Karl Michael Attard 10-01-2023 11:08:00

English (United Kingdom)

Page 25: [40] Formatted Karl Michael Attard 10-01-2023 11:08:00

English (United Kingdom)

Page 25: [41] Formatted Karl Michael Attard 10-01-2023 11:06:00

Centered

Page 25: [42] Formatted Table Karl Michael Attard 10-01-2023 11:16:00

Formatted Table

Page 25: [43] Formatted Karl Michael Attard 10-01-2023 11:08:00

English (United Kingdom)

Page 25: [44] Formatted Karl Michael Attard 10-01-2023 11:07:00

Centered

Page 25: [45] Formatted Karl Michael Attard 10-01-2023 11:08:00

English (United Kingdom)

Page 25: [46] Formatted Karl Michael Attard 10-01-2023 11:08:00

English (United Kingdom)

Page 25: [47] Formatted Karl Michael Attard 10-01-2023 11:08:00

Font: Italic, English (United Kingdom)

Page 25: [47] Formatted Karl Michael Attard 10-01-2023 11:08:00

Font: Italic, English (United Kingdom)

Page 25: [47] Formatted Karl Michael Attard 10-01-2023 11:08:00

Font: Italic, English (United Kingdom)

Page 25: [48] Formatted Karl Michael Attard 10-01-2023 11:08:00

English (United Kingdom)

Page 25: [48] Formatted Karl Michael Attard 10-01-2023 11:08:00

English (United Kingdom)

Page 25: [49] Formatted	Karl Michael Attard	10-01-2023 11:08:00
English (United Kingdom)		◀
▲		
Page 25: [50] Formatted	Karl Michael Attard	10-01-2023 11:07:00
Centered		◀
▲		
Page 25: [51] Formatted	Karl Michael Attard	10-01-2023 11:08:00
English (United Kingdom)		◀
▲		
Page 25: [51] Formatted	Karl Michael Attard	10-01-2023 11:08:00
English (United Kingdom)		◀
▲		
Page 25: [52] Formatted	Karl Michael Attard	10-01-2023 11:08:00
English (United Kingdom)		◀
▲		
Page 25: [52] Formatted	Karl Michael Attard	10-01-2023 11:08:00
English (United Kingdom)		◀
▲		
Page 25: [53] Formatted	Karl Michael Attard	10-01-2023 11:08:00
English (United Kingdom)		◀
▲		
Page 25: [54] Formatted	Karl Michael Attard	10-01-2023 11:08:00
English (United Kingdom)		◀
▲		
Page 25: [54] Formatted	Karl Michael Attard	10-01-2023 11:08:00
English (United Kingdom)		◀
▲		
Page 25: [55] Formatted	Karl Michael Attard	10-01-2023 11:08:00
English (United Kingdom)		◀
▲		
Page 25: [56] Formatted	Karl Michael Attard	10-01-2023 11:07:00
Centered		◀
▲		
Page 25: [57] Formatted	Karl Michael Attard	10-01-2023 11:08:00
English (United Kingdom)		◀
▲		
Page 25: [57] Formatted	Karl Michael Attard	10-01-2023 11:08:00
English (United Kingdom)		◀
▲		
Page 25: [58] Formatted	Karl Michael Attard	10-01-2023 11:08:00
English (United Kingdom)		◀
▲		
Page 25: [58] Formatted	Karl Michael Attard	10-01-2023 11:08:00
English (United Kingdom)		◀
▲		

Page 25: [59] Formatted	Karl Michael Attard	10-01-2023 11:08:00
English (United Kingdom)		◀
▲		
Page 25: [60] Formatted	Karl Michael Attard	10-01-2023 11:08:00
English (United Kingdom)		◀
▲		
Page 25: [60] Formatted	Karl Michael Attard	10-01-2023 11:08:00
English (United Kingdom)		◀
▲		
Page 25: [61] Formatted	Karl Michael Attard	10-01-2023 11:08:00
English (United Kingdom)		◀
▲		
Page 25: [62] Formatted	Karl Michael Attard	10-01-2023 11:07:00
Centered		◀
▲		
Page 25: [63] Formatted	Karl Michael Attard	10-01-2023 11:08:00
English (United Kingdom)		◀
▲		
Page 25: [63] Formatted	Karl Michael Attard	10-01-2023 11:08:00
English (United Kingdom)		◀
▲		
Page 25: [64] Formatted	Karl Michael Attard	10-01-2023 11:08:00
English (United Kingdom)		◀
▲		
Page 25: [64] Formatted	Karl Michael Attard	10-01-2023 11:08:00
English (United Kingdom)		◀
▲		
Page 25: [65] Formatted	Karl Michael Attard	10-01-2023 11:08:00
English (United Kingdom)		◀
▲		
Page 25: [66] Formatted	Karl Michael Attard	10-01-2023 11:08:00
English (United Kingdom)		◀
▲		
Page 25: [66] Formatted	Karl Michael Attard	10-01-2023 11:08:00
English (United Kingdom)		◀
▲		
Page 25: [67] Formatted	Karl Michael Attard	10-01-2023 11:08:00
English (United Kingdom)		◀
▲		
Page 25: [68] Formatted	Karl Michael Attard	10-01-2023 11:07:00
Centered		◀
▲		
Page 25: [69] Formatted	Karl Michael Attard	10-01-2023 11:08:00
English (United Kingdom)		◀
▲		

Page 25: [69] Formatted	Karl Michael Attard	10-01-2023 11:08:00
English (United Kingdom)		◀
▲		
Page 25: [70] Formatted	Karl Michael Attard	10-01-2023 11:08:00
English (United Kingdom)		◀
▲		
Page 25: [70] Formatted	Karl Michael Attard	10-01-2023 11:08:00
English (United Kingdom)		◀
▲		
Page 25: [71] Formatted	Karl Michael Attard	10-01-2023 11:08:00
English (United Kingdom)		◀
▲		
Page 25: [72] Formatted	Karl Michael Attard	10-01-2023 11:08:00
English (United Kingdom)		◀
▲		
Page 25: [72] Formatted	Karl Michael Attard	10-01-2023 11:08:00
English (United Kingdom)		◀
▲		
Page 25: [73] Formatted	Karl Michael Attard	10-01-2023 11:08:00
English (United Kingdom)		◀
▲		
Page 25: [74] Formatted	Karl Michael Attard	10-01-2023 11:17:00
English (United Kingdom)		◀
▲		
Page 25: [75] Formatted	Karl Michael Attard	10-01-2023 11:07:00
Centered		◀
▲		
Page 25: [76] Formatted	Karl Michael Attard	10-01-2023 11:08:00
English (United Kingdom)		◀
▲		
Page 25: [77] Formatted	Karl Michael Attard	10-01-2023 11:07:00
Centered		◀
▲		
Page 25: [78] Formatted	Karl Michael Attard	10-01-2023 11:08:00
English (United Kingdom)		◀
▲		
Page 25: [79] Formatted	Karl Michael Attard	10-01-2023 11:08:00
English (United Kingdom)		◀
▲		
Page 25: [80] Formatted	Karl Michael Attard	10-01-2023 11:08:00
Font: Italic, English (United Kingdom)		◀
▲		
Page 25: [80] Formatted	Karl Michael Attard	10-01-2023 11:08:00
Font: Italic, English (United Kingdom)		◀
▲		

Page 25: [80] Formatted Karl Michael Attard 10-01-2023 11:08:00

Font: Italic, English (United Kingdom)

Page 25: [81] Formatted Karl Michael Attard 10-01-2023 11:08:00

English (United Kingdom)

Page 25: [81] Formatted Karl Michael Attard 10-01-2023 11:08:00

English (United Kingdom)

Page 25: [82] Formatted Karl Michael Attard 10-01-2023 11:08:00

English (United Kingdom)

Page 25: [83] Formatted Karl Michael Attard 10-01-2023 11:08:00

Centered

Page 25: [84] Formatted Karl Michael Attard 10-01-2023 11:08:00

English (United Kingdom)

Page 25: [85] Formatted Karl Michael Attard 10-01-2023 11:08:00

English (United Kingdom)

Page 25: [86] Formatted Karl Michael Attard 10-01-2023 11:08:00

English (United Kingdom)

Page 25: [87] Formatted Karl Michael Attard 10-01-2023 11:08:00

Centered

Page 25: [88] Formatted Karl Michael Attard 10-01-2023 11:08:00

English (United Kingdom)

Page 25: [89] Formatted Karl Michael Attard 10-01-2023 11:08:00

English (United Kingdom)

Page 25: [89] Formatted Karl Michael Attard 10-01-2023 11:08:00

English (United Kingdom)

Page 25: [90] Formatted Karl Michael Attard 10-01-2023 11:08:00

English (United Kingdom)

Page 25: [91] Formatted Karl Michael Attard 10-01-2023 11:08:00

Centered

Page 25: [92] Formatted Karl Michael Attard 10-01-2023 11:08:00

English (United Kingdom)

Page 25: [93] Formatted	Karl Michael Attard	10-01-2023 11:08:00
English (United Kingdom)		◀-----
▲-----		
Page 25: [93] Formatted	Karl Michael Attard	10-01-2023 11:08:00
English (United Kingdom)		◀-----
▲-----		
Page 25: [94] Formatted	Karl Michael Attard	10-01-2023 11:08:00
English (United Kingdom)		◀-----
▲-----		
Page 25: [95] Formatted	Karl Michael Attard	10-01-2023 11:08:00
Centered		◀-----
▲-----		
Page 25: [96] Formatted	Karl Michael Attard	10-01-2023 11:08:00
English (United Kingdom)		◀-----
▲-----		
Page 25: [97] Formatted	Karl Michael Attard	10-01-2023 11:08:00
English (United Kingdom)		◀-----
▲-----		
Page 25: [98] Formatted	Karl Michael Attard	10-01-2023 11:08:00
English (United Kingdom)		◀-----
▲-----		
Page 25: [99] Formatted	Karl Michael Attard	10-01-2023 11:08:00
English (United Kingdom)		◀-----
▲-----		